

## ORIGINAL ARTICLE

# Osteohistological and taphonomic life-history assessment of *Edmontosaurus annectens* (Ornithischia: Hadrosauridae) from the Late Cretaceous (Maastrichtian) Ruth Mason dinosaur quarry, South Dakota, United States, with implication for ontogenetic segregation between juvenile and adult hadrosaurids

Mateusz Wosik<sup>1,2,3</sup>  | David C. Evans<sup>2,3</sup>

<sup>1</sup>Department of Biology, Misericordia University, Dallas, Pennsylvania, USA

<sup>2</sup>Department of Ecology and Evolutionary Biology, University of Toronto, Toronto, Ontario, Canada

<sup>3</sup>Department of Natural History, Royal Ontario Museum, Toronto, Ontario, Canada

## Correspondence

Mateusz Wosik, Department of Biology, Misericordia University, 301 Lake Street, Dallas, PA 18612, USA.  
Email: [mwosik@misericordia.edu](mailto:mwosik@misericordia.edu)

## Funding information

Dinosaur Research Institute, Grant/Award Number: Student Project Grant; Natural Sciences and Engineering Research Council of Canada, Grant/Award Number: Discovery Grant RGPIN 355845; University of Toronto, Grant/Award Number: Joseph Bazylewicz Fellowship, University of Toronto Fellowship and University of Toronto Research Assistantship

## Abstract

The Late Cretaceous (Maastrichtian) Ruth Mason Dinosaur Quarry (RMDQ) represents a monodominant *Edmontosaurus annectens* bonebed from the Hell Creek Formation of South Dakota and has been determined as a catastrophic death assemblage likely belonging to a single population, providing an ideal sample to investigate hadrosaurid growth and population dynamics. For this study, size-frequency distributions were constructed from linear measurements of long bones (humeri, femora, tibiae) from RMDQ that revealed five relatively distinct size classes along a generally right-skewed distribution, which is consistent with a catastrophic assemblage. To test the relationship between morphological size ranges and ontogenetic age classes, subsets from each size-frequency peak were transversely thin-sectioned at mid-diaphysis to conduct an ontogenetic age assessment based on growth marks and observations of the bone microstructure. When combining these independent datasets, growth marks aligned with size-frequency peaks, with the exclusion of the overlapping subadult-adult size range, indicating a strong size-age relationship in early ontogeny. A growth curve analysis of tibiae indicated that *E. annectens* exhibited a similar growth trajectory to the Campanian hadrosaurid *Maiasaura*, although attaining a much larger asymptotic body size by about 9 years of age, further suggesting that the clade as a whole may have inherited a similar growth strategy. This rich new dataset for *E. annectens* provides new perspectives on other hypotheses of hadrosaurid life history. When the RMDQ population was compared with size distributions from other hadrosaurid bonebed assemblages, juveniles (categorized as ages one and two) were either completely absent from or heavily underrepresented in the samples, providing support for the hypothesized segregation between juvenile and adult hadrosaurids. Osteohistological comparison with material from polar and temperate populations of *Edmontosaurus* revealed that previous conclusions correlating osteohistological growth patterns with the strength of environmental stressors were a result of sampling non-overlapping ontogenetic growth stages.

## KEYWORDS

annectens, bonebed, demography, dinosaur, duck bill, duck-billed, *Edmontosaurus*, growth, growth curve, growth marks, hadrosaur, hadrosaurid, Hell Creek Formation, histology, long bone, mass death assemblage, osteohistology, paleohistology, Ruth Mason, size-frequency, South Dakota, yearling

## 1 | INTRODUCTION

Osteohistology, the study of bone tissues, has been increasingly utilized in paleontological studies to reveal insights such as ontogenetic status, physiology, and annual bone deposition rates (e.g., Buffrenil et al., 2021; Francillon-Vieillot et al., 1990; Hall, 2015; Padian, 2013). This has provided information unobtainable from superficial morphology to attempt life-history reconstructions of extinct animals (e.g., Erickson et al., 2006; Erickson & Tumanova, 2000; Woodward et al., 2015), supported by observations of extant animals (e.g., Buffrenil & Castanet, 2000; Köhler et al., 2012; Woodward et al., 2011). Some of the most detailed studies of non-avian dinosaur osteohistological variability have been conducted on hadrosaurids (Horner et al., 1999, 2000; Woodward et al., 2015; Wosik et al., 2020). Horner et al. (2000) reconstructed a growth series of the hadrosaurid *Maiasaura peeblesorum* derived from contemporaneous nesting grounds, bonebeds, and isolated skeletons that would form a fundamental framework for future life-history analyses of fossil dinosaur taxa. From cross-sectional observations of growth marks (e.g., lines of arrested growth; LAGs) and patterns of bone tissue change, the authors established ontogenetic stages for relative size ranges across the complete lifespan of this taxon.

However, expansion and shape change of the medullary cavity due to biomechanical factors and physiological processes can obliterate growth marks representative of early ontogeny and result in underestimations of ontogenetic age (e.g., Cooper et al., 2008; Horner & Padian, 2004; Woodward et al., 2013). To account for this, growth marks from an ontogenetic series can be sequentially stacked, but this generally requires a growth series of the same element (Bybee et al., 2006; Chinsamy, 1993; Erickson et al., 2001). Alternatively, a quantitative model-fitting retrocalculation method was introduced by Cooper et al. (2008) that used a series of regression equations fit to plots of the measured circumferences of individual bones from *Hypacrosaurus* as a function of age to estimate the size of missing growth marks and has been demonstrated to be a more accurate measure than section-stacking (Chiba, 2018; Chiba et al., 2015). Lee and O'Connor (2013) later applied the retrocalculation method for the purpose of reconstructing growth rates. Taking these new methods into account, Woodward et al. (2015) expanded on the initial *Maiasaura* study by Horner et al. (2000) and integrated Developmental Mass Extrapolation (DME; Erickson & Tumanova, 2000) to produce the first body mass growth curve for a hadrosaurid, further establishing *Maiasaura* as the most ontogenetically well understood non-avian dinosaur.

The life-history synthesis from studies of *Maiasaura* (e.g., Horner & Makela, 1979; Horner, 1982; Varricchio & Horner, 1993; Barretto, 1997; Dilkes, 2000, 2001; Horner, 1999) has been broadly

extrapolated to the hadrosaurid clade with a relatively limited investigation into additional hadrosaurids despite an abundance of available material from numerous taxa. *Edmontosaurus* is one of the largest hadrosaurids with two currently recognized species, *E. annectens* and *E. regalis*, which are distinguished through subtle cranial morphologies and by their geographic distributions and temporal segregation (Campione & Evans, 2011; Xing et al., 2014, 2017). It is one of the best-sampled hadrosaurids known from over a dozen complete articulated skeletons across the entire ontogenetic sequence (Wosik, Goodwin, & Evans, 2017 and references therein; Farke and Yip, 2019) and multiple monodominant bonebeds that preserve a wide spectrum of ontogenetic stages and population samples (Bell & Campione, 2014; Christians, 1992; Colson et al., 2004; Evans et al., 2015; Gangloff & Fiorillo, 2010; Ullmann et al., 2017; Snyder et al., 2020). The current fossil record of *Edmontosaurus* thus preserves one of the most extensive ontogenetic samples for any dinosaurian taxon, making it ideal for life-history studies of a fossil organism, even at the population level.

In this study, we conducted an ontogenetic osteohistological assessment of *Edmontosaurus annectens* from the Late Cretaceous (Maastrichtian, ~66–67 mya) Ruth Mason Dinosaur Quarry (RMDQ), Hell Creek Formation of South Dakota, United States. The extensive preservation (>10,000 bones) of this monodominant *E. annectens* bonebed (Christians, 1992) allowed us to independently evaluate hadrosaurid growth and population dynamics, and because of the non-selective nature of this catastrophic mass death assemblage (Christians, 1992), representatives across ontogeny were preserved, presumably in proportions equivalent to the living population's age structure (Olson, 1957). The primary goals of this study were to (1) describe the ontogenetic osteohistological changes in the major limb bones of *E. annectens*, (2) reconstruct the growth rate and population structure of *E. annectens*, and (3) further assess the potential of using size-frequency distributions as a proxy for ontogenetic age in hadrosaurids (Brinkman, 2014; Wosik et al., 2020). In addition, this study also supplied a key reference point for reevaluating the suggested relationship between osteohistological patterns and environmental stressors in *Edmontosaurus* (Chinsamy et al., 2012; Vanderven et al., 2014).

## 2 | GEOLOGICAL SETTING

The Ruth Mason Dinosaur Quarry (RMDQ) is a monodominant *E. annectens* bonebed consisting of over 10,000 disarticulated bones of this taxon from the Hell Creek Formation (Late Cretaceous: upper Maastrichtian, ~66–67 million years ago). It is located in Ziebach County, South Dakota (Figure 1) and was first discovered in the



**FIGURE 1** Geographic maps of the United States (a) and South Dakota (b) denoting the location of the Ruth Mason dinosaur quarry (RMDQ)

early 1900s by Ruth Mason. The RMDQ lies in the southern part of the Williston Basin and strata from the Maastrichtian aged Fox Hills and Hell Creek formations are both visibly exposed in the area (Christians, 1992).

Based on data from taphonomic analyses (Christians, 1992), the RMDQ was considered a pauci-specific, parautochthonous assemblage dominated by the disarticulated remains of *E. annectens*. Strong evidence of size-frequency profiles and limited subaerial exposure prior to burial based on uniform 'stage 0' weathering (Behrensmeyer, 1978) of cranial and postcranial elements suggest a mass death of several hundred to perhaps thousands of *E. annectens* individuals (Christians, 1992). Results from sedimentological analyses of the deposit demonstrated that the bone horizon recorded at least two depositional events. The lower half is indicative of a debris flow, identified through randomly oriented and upended bones comprising a poorly sorted and crudely graded assemblage of freshwater, fluvial fauna, in addition to the dinosaurian remains (Christians, 1992). The upper half represents a characteristic floodplain deposit containing randomly distributed remains of terrestrial and freshwater organisms with strong similarities to fauna of the lower half. The unique combination of the taphonomic and sedimentologic data exemplifies a catastrophic death assemblage characteristic of a debris flow that was secondarily redeposited locally (Christians, 1992).

The RMDQ has been excavated since 1979 by multiple institutions (Black Hills Institute of Geological Research [BHI], University of Wisconsin-Madison [UWGM], University of Chicago, and The Children's Museum of Indianapolis [TCM]) and has been subjected to varying degrees of excavation. Both BHI and TCM, from which the majority of specimens from our dataset originate, instituted

exhaustive excavation protocols that significantly reduced biases related to collection (e.g., small vs. large, complete vs. incomplete). Detailed locality information of each specimen is on file at its respective institution.

### 3 | MATERIALS AND METHODS

The sample size of *E. annectens* long bones from the RMDQ consisted of a total of 639 specimens across all six major limb elements: femora 155, tibiae 130, fibulae 108, humeri 103, radii 82, and ulnae 61. In addition, 270 metacarpals and metatarsals were collectively analyzed as a taphonomic proxy for smaller limbs. All available bone elements were used for each respective analysis to attempt to capture a more accurate representation of the original standing crop and due to the assemblage's secondary redeposition, which is detailed in the previous section regarding the geological setting. To construct the initial size-frequency distributions, measurement data was gathered from recorded field collection logs (Table S1), which are permanently accessioned at the Royal Ontario Museum. Over 85% of the specimens included in this study have been personally seen and measured (MW) to verify the correct identification of each bone and its field measurement. Size-frequency distributions were updated to account for minor discrepancies. Specimens used for osteohistological sampling (Table 1) were then selected from each size-frequency peak, which were excavated by BHI between 1979 and 1991 prior to acquisition by the Royal Ontario Museum in 2014–2016. Completeness of bones was identified on the basis of general preservation and ability to obtain both the total length and minimum diaphyseal circumference measurements, and was categorized as complete, nearly complete,

**TABLE 1** List of *Edmontosaurus* specimens osteohistologically sampled and examined for this study and their corresponding measurement values. % RMDQ represents the ratio of the specimen to the largest corresponding element from RMDQ

Element	Specimen	Size-class	Total length	% RMDQ	Circumference	% RMDQ	MinA	MaxA	MCmin	MCmax	MC%	Preserved GM circs
Humerus	ROM 73849	Late juvenile	375	54.5	136	51.5	32.3	47.8	18.5	31.3	37.5	
	ROM 67796	Early subadult	452*	70.0	173	65.5	52.0	59.0	34.0	41.0	45.4	143, 167
	ROM 73850	Late subadult	520	76.0	208	78.5	54.0	72.0	27.0	50.0	34.7	147, 173, 186
	ROM 67794	Late adult	650	95.0	240	90.5	69.0	85.0	40.0	54.0	36.8	179, 196, 216, 227, 237, 239, 241, 242, 243, 244, 245
Femur	ROM 67602	Late juvenile	675	55.0	255	53.5	67.0	87.5	41.0	48.0	33.6	
	ROM 67798	Late juvenile	704.5*	57.0	256	54.0	74.0	84.0	42.0	49.0	33.1	227
	ROM 67799	Early subadult	865	70.5	318	67.0	98.0	104.0	76.0	79.0	58.9	272, 297
	ROM 67792	Early adult	1065	86.5	410	86.5	98.0	104.0	72.0	96.0	67.8	330, 367.5, 385
Tibia	ROM 67603	Late juvenile	555	53.5	184.5	51.5	57.0	58.0	30.0	30.0	27.2	
	ROM 67601	Late juvenile	575	55.5	194	54.0	54.0	61.0	25.0	32.0	24.3	
	ROM 67797	Early subadult	677*	65.0	233	65.0	65.0	79.0	29.0	49.0	27.7	196.5
	ROM 67795	Early subadult	720	69.0	237.5	66.0	72.0	73.0	33.0	37.0	23.2	202
	ROM 67793	Early adult	875	84.0	275	76.5	80.0	85.0	38.0	42.0	23.5	213, 249
	ROM 73852	Late adult	1030	99.0	350	97.0	104.0	115.5	47.5	52.0	20.6	197, 236.5, 259.5, 274.5, 302, 318, 326.5, 332, 335, 336, 336.5, 337.5
ROM 73853	Late adult	1025	98.5	360	100.0	106.0	116.5	56.0	56.0	25.4	212.5, 254.5, 282, 309.5, 329, 334.5, 338.5, 340.5, 342.75, 344, 345, 347, 349, 350, 351.5, 352.2, 353, 354	

\*Estimated based on OLS regression using the respective circumference data.

Abbreviations: GM, growth mark; MaxA, major axis diameter; MCmax, medullary cavity diameter along the major axis; MCmin, medullary cavity diameter along the minor axis; MC%, ratio between the cross-sectional areas of the medullary cavity and outer circumference; MinA, minor axis diameter.

and incomplete. Linear measurements under 30 cm were taken with digital calipers, while those over 30 cm and all circumferences were taken using a fabric tape measure. Categorization of specimens followed published ontogenetic stages of the closely related hadrosaurid dinosaur *M. peeblesorum*, recognized on the basis of relative size, patterns of histological changes, and associations with eggs and nests (Horner et al., 2000), and were then proportionately adjusted to account for the relatively larger size of *Edmontosaurus* at each ontogenetic stage (Wosik, Goodwin, & Evans, 2017).

### 3.1 | Regression analyses

In order to maximize sample sizes for size-frequency distributions, Ordinary Least Squares (OLS) regressions between the total length and minimum diaphyseal circumference of complete humeri, femora, and tibiae from the entire RMDQ dataset of each respective major limb element were used to estimate the size of the corresponding variable for incomplete elements. The purpose of this was to include valuable data from incompletely preserved or obstructed (e.g., half jackets) specimens and subsequently increase the overall sample size. This procedure was not performed on radii, ulnae, and fibulae because the minimum diaphyseal circumference can significantly vary ontogenetically along the proximal-distal axis (personal observation) and would introduce bias unless properly controlled. Linear data were log-transformed prior to analysis using natural log (ln). Slopes, intercepts, 95% confidence intervals, and correlation coefficients were determined for each comparison. Each comparison was then evaluated using two-tailed *p*-values using a significance level of 0.05 for correlation between variables. The regressions and statistical analyses were performed in R (R-Development-Core-Team, 2016) with the package lmodel2 (Lengendre, 2013).

### 3.2 | Size-frequency distributions

Individual size-frequency distributions of total length and minimum diaphyseal circumference were generated in R (R-Development-Core-Team, 2016) using the entire dataset for humeri, femora, and tibiae, whereas only total length was analyzed for ulnae, radii, and fibulae. For relative scale, the largest corresponding element from RMDQ was used to represent a presumably morphologically adult-sized specimen of *E. annectens*, which was verified by histology. Combined size-frequency distributions consisted of data from humeri, femora, and tibiae. In addition, a collective size-frequency distribution of metacarpals and metatarsals was generated to test whether nestling and early juvenile individuals, whose limb bones were hydraulically similar, were sorted out taphonomically. To determine whether our size-frequency distributions were sensitive to size and the amount of bins, we attempted to optimize these values using the method of Shimazaki and Shinomoto (2007, 2010). The resulting range of values was then utilized as a guideline when applying the broken stick method to each individual size-frequency distribution. A general average of approximately 25

bins was determined to be optimal among the size-frequency distributions. A similar approach was taken in Wosik et al. (2020).

### 3.3 | Osteohistology

In order to generate a growth curve and assess growth rate variation, a total of 15 RMDQ specimens consisting of four humeri, four femora, and seven tibiae from the Royal Ontario Museum (ROM) collections were histologically thin-sectioned at the minimum diaphyseal circumference (see Table 1 for list of sampled specimens). Specimens for histological sectioning were selected from each size-frequency peak based on outer circumference to assess the correlation between size and age. Thin sections were made and imaged at the ROM Palaeohistology Laboratory, and all molding and casting materials and thin-sections are deposited at the ROM. Histological terminology follows that of Francillon-Vieillot et al. (1990). Cross-polarized filters were used to diagnose the orientation of collagen fibers (e.g., lamellar, parallel-fibered, woven-fibered). Vascular orientation is used to describe how the long axes of vascular canals are oriented in the bone matrix (e.g., longitudinal, radial, reticular, plexiform, laminar). Cyclical growth marks were diagnosed based on a variation or pause in the rate of bone growth and were used to determine the age and growth rates of sampled individuals. Lines of arrested growth (LAGs), a type of cyclical growth mark, were identified based on an attenuation or complete cessation in bone deposition, which would be visible along the circumference of the section. A zone represented the bone deposition region in between growth marks.

#### 3.3.1 | Thin-sectioning protocol

Prior to sectioning, specimens were mechanically prepared with pneumatic and hand tools to remove the surrounding rock matrix. Each specimen was measured and photographed, and three-dimensional models were generated using Agisoft PhotoScan. Complete cross-sectional thin-sections were produced using the standard fossil histology techniques (e.g., Lamm, 2013) as a guideline and modified as necessary to the requirements of the specimen and/or available equipment. Complete cross-sectional pucks including the minimum diaphyseal circumference were cut out using a Well diamond-plated wire saw or Buehler IsoMet 1000 Precision Cutter low-speed saw depending on the size of the specimen. The pucks were molded and cast, and the casts were then reinserted into the original bone. The pucks were completely embedded in Castolite polyester resin, cut on a Buehler IsoMet 1000 Precision Cutter low-speed saw, and mounted on 2–3 mm plexi-glass slides with PSI 122/124 resin. The blocks were then cut off the slides on the IsoMet, and the slides were subsequently ground down to the appropriate thickness to view overall bone microstructure using either a Hillquist Thin Sectioning Machine or grinding lap wheel. Slides were finished by hand polishing on a glass plate with 600 followed by 1000 silicon carbide grit and briefly placed into a sonic-bath to further remove any remaining grit and debris before imaging.

### 3.3.2 | Imaging protocol

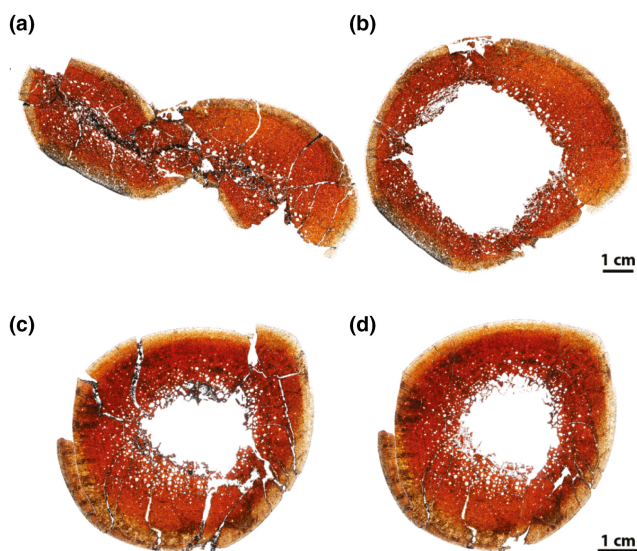
Images of thin-sections were captured using a Nikon DS-Fi1 camera mounted to a Nikon AZ-100 microscope under plain-polarized and cross-polarized light. Images were processed and assembled using Nikon NIS-Elements Basic Research 3.13 imaging software. Images were taken at variable magnifications dependent on specimen size, 1280×960 resolution, 2.9–8ms exposure, and set on dynamic contrast with 35%–40% overlap. Johnson & Johnson baby oil was added to each slide to increase the refraction index for clarity during imaging. Multiple images were taken for slides that exceeded the focal dimensions of the imaging stage and were later stitched together using the Automate>Photomerge feature in Adobe Photoshop. Further processing of images (e.g., text, scale bars) and retrodeformation was completed using Adobe Photoshop and Adobe Illustrator. Retrodeformation, which is the digital reconstruction of histological thin-sections, was performed to better recover a more accurate size and shape of the cross-sectional samples (Figure 2). This is an important step that is often overlooked when determining whether gaps along the circumference are indeed due to missing pieces of bone and/or a result of distortion from taphonomic processes, particularly in the case of lateral compression. The degree to which this process was required was dependent on the level of preservation of each specimen.

### 3.4 | Age determination and growth modeling

In order to account for the entire growth history, age retrocalculation (Cooper et al., 2008) was performed on tibiae with the longest growth record (ROM 73852; ROM 73853) to identify any potentially missing growth marks, or growth years. Retrocalculation and growth modeling were restricted to tibiae so our data could be compared

with previously published growth rates of other hadrosaurids (Cooper et al., 2008; Freedman Fowler & Horner, 2015; Woodward et al., 2015; Wosik et al., 2020). Tibia circumference and body mass growth curves were individually generated for these two tibiae, as well as a combined dataset of all recorded tibial growth marks using Richards-family growth models (Lee & O'Connor, 2013) in R (R-Development-Core-Team, 2016). Corrected Akaike Information Criterion ( $AIC_c$ ) values were used to account for small sample sizes using R package MuMIn (Bartoń, 2017). Next, delta  $AIC_c$  ( $\Delta AIC_c$ ) and  $AIC_c$  weight values were calculated to obtain averaged models for each specimen (Burnham & Anderson, 2002). Obtaining an averaged model is important when  $AIC_c$  values of individual models are within 10  $\Delta AIC_c$ , which deems each individual model as plausible (Burnham & Anderson, 2002). Finally, the retrocalculated ages obtained from the averaged model for the combined dataset were considered as the precise age of growth marks and applied in the tibia circumference and body mass growth curve analyses. An estimated yearling tibial circumference of 100mm was required to calibrate the curve at the early ontogenetic stage (Chiba et al., 2015), and this was obtained by using the recorded yearling growth mark of a hadrosaurid from the Dinosaur Park Formation (Wosik et al., 2020) and applying the proportionate difference between *Maiasaura* and *Edmontosaurus* nestlings (Wosik, Goodwin, & Evans, 2017). This was done because the retrocalculation on the individual tibiae was estimating growth years that were not present in the histological record, even in the younger individuals where secondary osteon development was very minimal, if present, in the cortical bone. An osteohistologically determined tibial hatchling circumference of 25 mm was used for each age retrocalculation model (Wosik et al., 2018; Wosik, Whitney, et al., 2017). Age was also cross-checked via section-stacking (Bybee et al., 2006) of growth marks, or annuli, from the histological samples in this study whenever possible. Transverse section periosteal surfaces (outer circumference) and circumferences of growth marks were traced in Adobe Illustrator. Data for tibiae of hadrosaurids used for comparison were obtained from Wosik et al., 2020.

An interspecific equation for quadrupedal vertebrates (Equation 1 of Campione & Evans, 2012) was used to estimate the body mass of SM R4050, which has a femur circumference of 460mm. This specimen was selected to represent a presumably morphologically adult individual for growth modeling rather than the holotype, USNM 2414, because it is the largest irrefutable associated skeleton of *E. annectens* that preserves complete and unobstructed circumferences for humeri and femora, which are required parameters for the interspecific equation. Developmental Mass Extrapolation (DME) (Erickson & Tumanova, 2000) was then used to convert tibial growth mark circumferences to body mass to account for deviations from the body mass equation for juvenile individuals.



**FIGURE 2** Examples of retrodeformation of RMDQ transverse cross sections. (a, b) Femur (ROM 67798). (c, d) Tibia (ROM 67603). (a, c) Unaltered. (b, d) Retrodeformed

## 4 | RESULTS

The level of preservation varied among the bone elements (e.g., humerus vs. tibia), which were preserved in a soft but iron-rich matrix

that could be particularly seen around the terminal ends. In rare cases, extensive pyritization had formed in the medullary cavity. All femora exhibited a high degree of lateral compression, especially along the shaft region. Despite this extensive crushing, the femoral head, trochanters, and distal condyles preserved their natural shapes in each individual, along with clear signs of articular cartilage attachments in larger individuals. Humeri were less compressed than the femora, but occasionally distorted in a spiral manner along the proximal-distal axis with the deltopectoral crest folding in on itself. Larger individuals better preserved the natural shape of the humerus, whereas smaller individuals would often have both an eroded humeral head and distal condyles or completely lacked one or both of their terminal ends. Tibiae were generally well preserved, with only a few cases of minor spiral torsion along the shafts. This taphonomic variability may have resulted from the stylopodial elements having larger medullary cavities relative to the cortical bone thickness, rendering them to be more prone to crushing than the dense tibiae. However, the proximal ends were consistently weathered or compressed, making the distinction between condyles more difficult if the cnemial crest was not clearly preserved. Despite these differences, nearly all bones preserved a beautiful glossy texture on the periosteal surface regardless of size, indicating that little, if any, of the periosteal surface was missing or had eroded/weathered away.

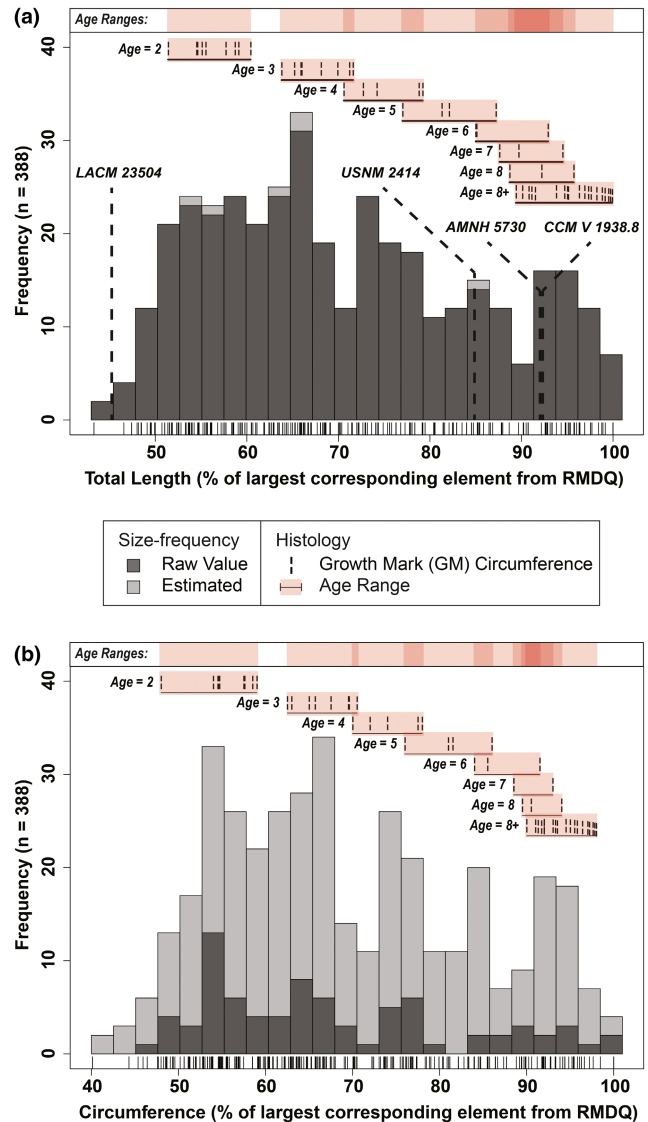
Of the 639 limb bones from the RMDQ analyzed in this study (Table S1), 626 (~98%) had measurable complete total lengths. The humerus sample consisted of 103 bones, of which 103 and 34 had measurable complete total lengths and minimum diaphyseal circumferences, respectively. Only 31 humeri had both variables that were measurable because a large portion of the sample was in half jackets, and therefore, obstructed circumference measurements. The femur sample consisted of 155 bones, of which 154 and 17 had measurable complete total lengths and minimum diaphyseal circumferences, respectively, and only 16 had both variables that were measurable. The tibia sample consisted of 130 bones, of which 129 and 28 had measurable complete total lengths and minimum diaphyseal circumferences, respectively, and 27 had both variables that were measurable. The remaining elements were only analyzed in terms of total length.

#### 4.1 | Regression analyses

Sample sizes of the OLS regression analyses (Table S2) ranged from 16 (femur) to 31 (humerus) individually complete specimens. All comparisons presented high coefficients of determination ( $R^2 > 0.94$ ) and significant correlation between variables based on low  $p$ -values ( $p < 8.47e^{-10}$ ). Therefore, estimation of incomplete elements could be confidently executed using the corresponding OLS regression values.

#### 4.2 | Size-frequency distributions

The combined total length size-frequency distribution (Figure 3a) consisted of a combined total of 388 humeri, femora, and tibiae and



**FIGURE 3** Combined size-frequency distributions comprised of humeri, femora, and tibiae from RMDQ with integrated osteohistological data. Tick marks below each distribution correspond with individual bones. (a) Total length with overlaid femur lengths from several associated skeletons of *Edmontosaurus annectens* (Wosik, Goodwin, & Evans, 2017). (b) Circumference.  $N = 388$ . Estimated values based on an ordinary least squares regression between total length and circumference (Table S2)

revealed five relatively distinct size-frequency peaks along a right-skewed distribution. The smallest size class, which resembled more of a broad cluster than a peak, included 110 individuals that ranged from ~43% to 60% of the linear dimensions of the largest corresponding element length from RMDQ, with a general concentration in the ~50%–60% size range. Articular surfaces were well defined when preserved and there were no signs of a porous periosteal surface, which instead exhibited a distinct sheen when fully prepared. Individuals in this size class would have had a body length ranging from 516 to 720 cm and corresponded with the late juvenile size class as defined in Horner et al. (2000) and proportionately adjusted for *Edmontosaurus* (Wosik, Goodwin, & Evans, 2017). The second size

class consisted of 77 subadult individuals that ranged from ~62% to 70%, with a very distinct size-frequency peak in the ~65%–67% size range, and would have corresponded with body lengths of 780–840 cm. The external morphology was similar to the late juvenile individuals except that attachment sites for muscles such as that along the fourth trochanter of the femur were much more defined. The third size class consisted of 61 subadult individuals that ranged from ~72%–79%. Using these data, the inclusive subadult size class of Horner et al. (2000) and Wosik, Goodwin, and Evans (2017) was split into two separate subadult size classes: early/small and late/large. Although we note that using early/late and small/large may not consider potential differences in size between sexes and intraspecific variation in growth, these terms were used to follow the convention of currently established categorizations (Horner et al., 2000; Wosik, Goodwin, & Evans, 2017) until more data are available to better refine the system. The fourth size class consisted of 39 adult individuals that ranged from ~82% to 89% with body lengths ranging between 984 and 1068 cm. Periosteal surface textures were very smooth and emitted a natural sheen, muscle attachment sites were substantially robust and showed extensive signs of scarring, and terminal epiphyseal surfaces were fully developed with large rugosities for articular cartilage attachments. The fifth size class consisted of 51 adult individuals that ranged in size from ~91% to 100%, which translated to individuals ~11–12 m in body length, exceeding any currently estimated *E. annectens* skeleton (Wosik, Goodwin, & Evans, 2017). In a similar fashion to the inclusive subadult size class, the inclusive adult size class presented here was split into early/small and late/large constituents.

The combined minimum diaphyseal circumference size-frequency distribution (Figure 3b) reflected the results of the combined total length size-frequency distribution with the general trend exhibiting a right skewed pattern where there was a progressive decrease between each proceeding size class. Size classes from the combined minimum diaphyseal circumference size-frequency distribution presented minor variations in their size ranges from those of the total length size-frequency distribution. When the dataset for the combined size-frequency distributions was partitioned into individual elements (Figures 4 and 5) for total length and minimum diaphyseal circumference, it was not possible to accurately discern the distinct boundaries between size classes (i.e., where one size class ended and another began). Although size-frequency peaks were recognizable in each size-frequency distribution, the amount of size-frequency peaks was not consistent among all the individual size-frequency distributions. However, the generally right-skewed trend as seen in the combined size-frequency distributions was apparent among all elements except for the ulna, which had the smallest sample size ( $n = 61$ ).

When superimposing associated skeletons, the late juvenile LACM 23504 consistently placed either within or just before the first size class (late juvenile) in all of the size-frequency distributions. The largest skeletons, AMNH 5730 and CCM V 1938.8 (both referred to *Anatotitan* [sensu Brett-Surman, 1989]), placed within the late adults among all six total length size-frequency distributions.

However, these same skeletons placed beyond the largest RMDQ minimum diaphyseal circumferences, suggesting that there may be a source of bias offsetting the circumference results or that the reported circumference measurements of the selected associated skeletons may be inaccurate. The offset could also be reflecting differences between growth strategies, but it is more likely to be an artifact of crushing in the RMDQ assemblage.

Curiously, the minimum extent for both of the combined size-frequency distributions was about 40% of the largest corresponding element from RMDQ. Therefore, a size-frequency distribution of autopodial elements (metacarpals and metatarsals) was generated to provide a basis for testing whether the size range of nestling to juvenile individuals, whose limb bones were hydraulically similar to the autopodial elements, were transported out taphonomically via hydraulic action. When superimposing associated skeletons of *E. annectens* on the collective size-frequency distribution of metacarpal and metatarsal total lengths (Figure 6), the metatarsal III of the late juvenile LACM 23504 placed at the leftmost extent of the metatarsals from RMD. But most importantly, femur lengths of nestlings from *E. annectens* (UCMP 128181) (Wosik, Goodwin, & Evans, 2017) and *Maiasaura* (YPM-PU 22432; YPM-PU 22400) (Horner et al., 2000) placed well within the left tail of the size-frequency distribution that consisted of ~38 equivalently sized autopodial elements.

### 4.3 | Osteohistology

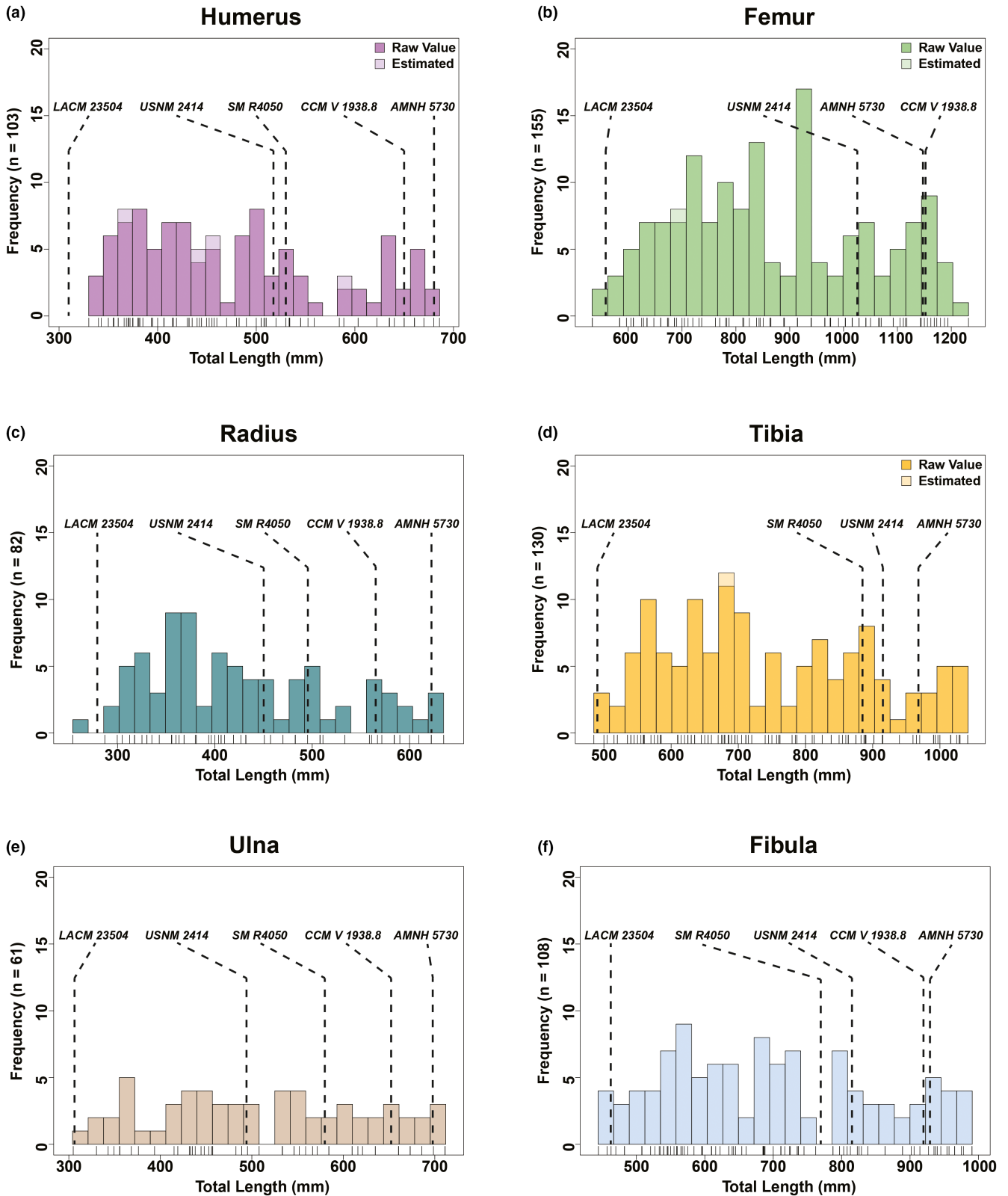
All osteohistologically sampled specimens are preserved in complete cross sections and are listed in Table 1. Categorization of specimens followed published ontogenetic stages for hadrosaurids (Horner et al., 2000; Wosik, Goodwin, & Evans, 2017) and was further split using the size-frequency distribution data presented herein. Five growth stages were recognized with the RMDQ sample: late juveniles, early subadults, late subadults, early adults, and late adults. As mentioned above, we understand that early/late and small/large may not account for potential differences in size between sexes and intraspecific variation in growth. However, these terms were tentatively used to follow the convention of currently established categorizations (Horner et al., 2000; Wosik, Goodwin, & Evans, 2017) until more data are available to better refine the system. The osteohistology of forelimb elements (humerus) is presented first and followed by elements of the hind limb (femur, tibia). Each element is then separated into size classes.

#### 4.3.1 | Humerus

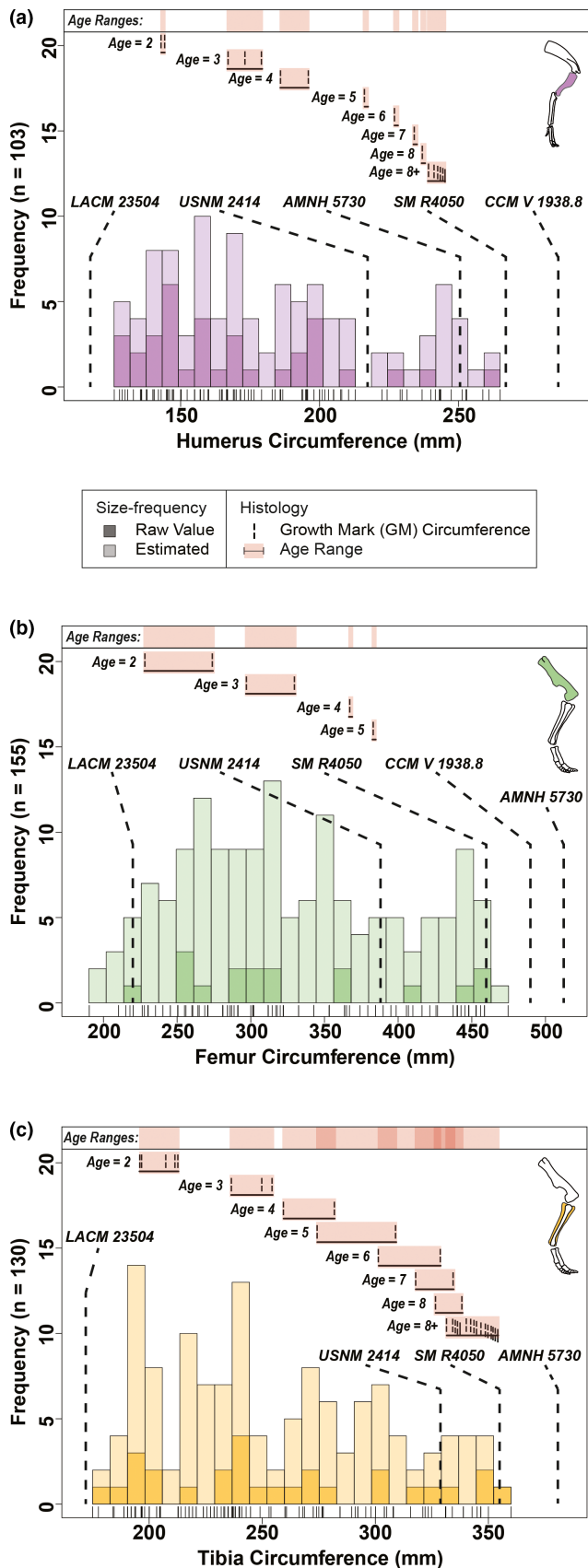
##### *Late juvenile*

Specimen examined: ROM 73849 (Figure 7a,b). The mid-diaphyseal perimeter was elliptical in cross section but was slightly crushed. An identical pattern was reflected in the shape of the medullary cavity, which was substantially cancellous with very large cancellous spaces relative to the cortical bone, and constituted 37.5% of the surface





**FIGURE 4** Total length size-frequency distributions of individual long bone elements from the Ruth Mason dinosaur quarry. Tick marks below each distribution correspond with individual bones. Estimated values based on an ordinary least squares regression between total length and circumference (Table S2)



**FIGURE 5** Circumference size-frequency distributions of individual long bone elements from the Ruth Mason dinosaur quarry with integrated osteohistological data. Outer circumferences from several associated skeletons of *Edmontosaurus annectens* (Wosik, Goodwin, & Evans, 2017) are overlaid in each size-frequency distribution. Tick marks below each distribution correspond with individual bones. (a) Humerus ( $n = 103$ ). (b) Femur ( $n = 155$ ). (c) Tibia ( $n = 130$ ). Estimated values based on an ordinary least squares regression between total length and circumference (Table S2). Skeletal reconstructions by D. Dufault

compact bone was not identifiable. The cortical bone, or compacta, was composed of primary bone tissues with reticular vascular canal orientation that, going outwards, shifted into plexiform and finally into a sub-laminar, or nearly circumferential, orientation at the periosteal surface. The main component of the compacta was parallel-fibered bone, which was highly isotropic, with some instances of woven-fibered bone particularly at the interface between the cortical bone and the medullary cavity. There were no signs of growth marks or secondary osteon development but enlarged resorption cavities were present within the medullary cavity and inner cortex regions.

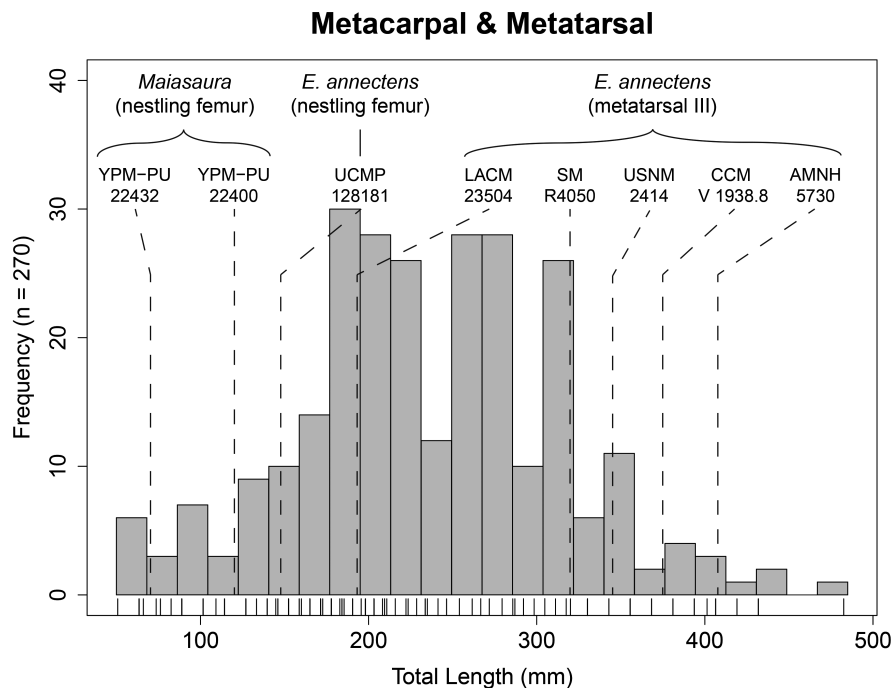
*Early subadult*

Specimen examined: ROM 67796 (Figure 7c,d). When retrodeformed (Figure 2), the mid-diaphyseal perimeter resembled a triangular-like shape with well-rounded corners and convex edges. The medullary cavity, which constituted 45.4% of the cross-sectional area, reflected the triangular shape of the periosteal perimeter and was more cancellous with larger vascular canal spaces than the late juvenile (ROM 73849). Fibrolamellar bone, defined as a “complex of woven-fibered scaffolding with intervening primary osteons of varying orientations” (Huttenlocker et al., 2013), comprised the majority of the medullary cavity bone tissues; under cross-polarized light, erosional cavities were lined with dense lamellar bone in which the collagen fibrils alternated their depositional direction between concentric layers. An endosteal margin of the compact bone was not identifiable, a likely result of the expanding medullary cavity. The cortical bone was composed of primary parallel-fibered bone tissues with several zones of vascular canals shifting from plexiform to laminar orientation. Between each zone was a cyclical growth mark, or annulus, similar to those observed in *Maiasaura* (Woodward et al., 2015), in that a clear cessation in bone deposition was not visible but instead consisted of a narrow transition of parallel-fibered/lamellar bone with weakly anastomosing vascular canals; two such growth marks were present with a third beginning to develop at the periosteal surface, as evidenced by the layering of parallel-fibered bone with laminar vascular canal orientation. Varying sizes of secondary osteons each with a distinct cement line were scattered throughout the medullary cavity region and began to invade the interface between the cortical bone and the medullary cavity.

*Late subadult*

Specimen examined: ROM 73850 (Figure 7e,f). The mid-diaphyseal perimeter resembled the triangular-like shape of the early subadult (ROM 67796), but the edge corresponding with the medial side of

area of the entire cross section. The inner cortex was largely composed of highly disorganized woven-fibered bone based on its anisotropic pattern under cross-polarized light; an endosteal margin of the



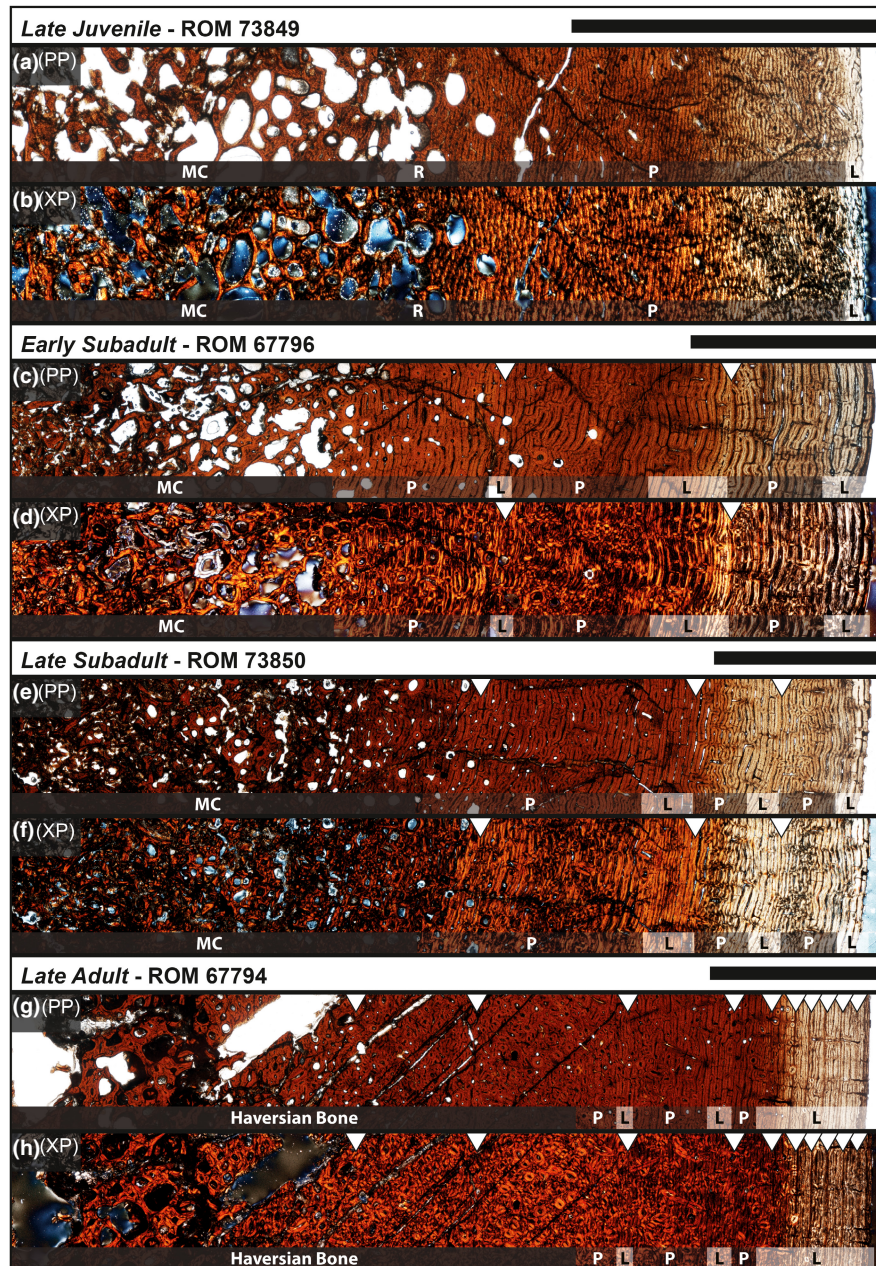
**FIGURE 6** Combined total length size-frequency distribution of metacarpals and metatarsals from the Ruth Mason dinosaur quarry. Tick marks below each distribution correspond with individual bones. Measurements for *Edmontosaurus annectens* metatarsal III and nestling femur length were obtained from Wosik, Goodwin, and Evans (2017), whereas those for *Maiasaura* nestlings originated from Horner et al. (2000).  $N = 270$

the bone was substantially flattened, and as a result, elongated the cross-sectional antero-posteriorly. The medullary cavity formed an elliptical shape that constituted only 34.7% of the cross-sectional area and had a similar degree of cancellous bone as the late juvenile (ROM 73849). Fibrolamellar bone comprised the majority of the medullary cavity bone tissues as well as the interface leading up to the cortical bone. The cortical bone was composed of primary parallel-fibered bone tissues with several zones of vascular canals shifting from plexiform to laminar orientation. Three growth marks, similar to those observed in the early subadult (ROM 67796), were present separating each zone with laminar vascular canal orientation. Closest to the periosteal surface, there was a more prominent layering of parallel-fibered/lamellar bone with laminar vascular canal orientation. Secondary osteons with multiple cement lines had fully invaded the cortical bone up to about the first growth mark (147 mm) and were slightly scattered within the next zone up to the second growth mark (173 mm). A Haversian system of overlapping generations of secondary osteons (Reid, 1985) was beginning to develop along the lateral side of the humerus at the interface between the medullary cavity and cortical bone.

#### Late adult

Specimen examined: ROM 67794 (Figure 7g,h). The mid-diaphyseal perimeter reflected the same shape of the late subadult (ROM 73850) but was more elongated antero-posteriorly. The medullary cavity formed an elliptical shape that constituted 36.8% of the cross-sectional area, similar to the late juvenile and late subadult stages.

The core of the medullary cavity was not preserved and left a large vacant space void of any matrix. The remainder of the medullary cavity was completely obliterated by multi-generational Haversian bone systems (Reid, 1985) that extended into the cortical bone up to about the third growth mark (216 mm). Although this level of secondary remodeling had obscured portions of the two preceding growth marks (179 and 196 mm), enough of each was identifiable in other regions of the cross section to accurately piece together the two respective circumferences. Therefore, the first two growth marks are marked for reference (Figure 7g,h). The cortical bone after the third growth mark was composed of a lamellar bone matrix that occasionally transitioned between parallel-fibered bone. Each zone primarily consisted of laminar vascular canal orientation with narrow regions of plexiform orientation. Secondary osteons, each with a single cement line, were scattered throughout the remainder of the cortex and were occasionally present near the periosteal surface. The sixth growth mark (239 mm) exhibited a clear cessation in bone deposition, as evidenced by an uninterrupted line around the entire circumference of the bone section, and was defined as the first LAG. The six LAGs that followed alternated between a similarly uninterrupted line and/or a semi-translucent opaque band within a lamellar bone matrix that consisted of very tightly stacked laminar vascular canals; these final six LAGs potentially resemble the onset of an external fundamental system (EFS; Horner et al., 2000) or outer circumferential layer (OCL; Chinsamy-Turan, 2005), which have been interpreted to signal skeletal maturity (Horner et al., 2000; Chinsamy-Turan, 2005).



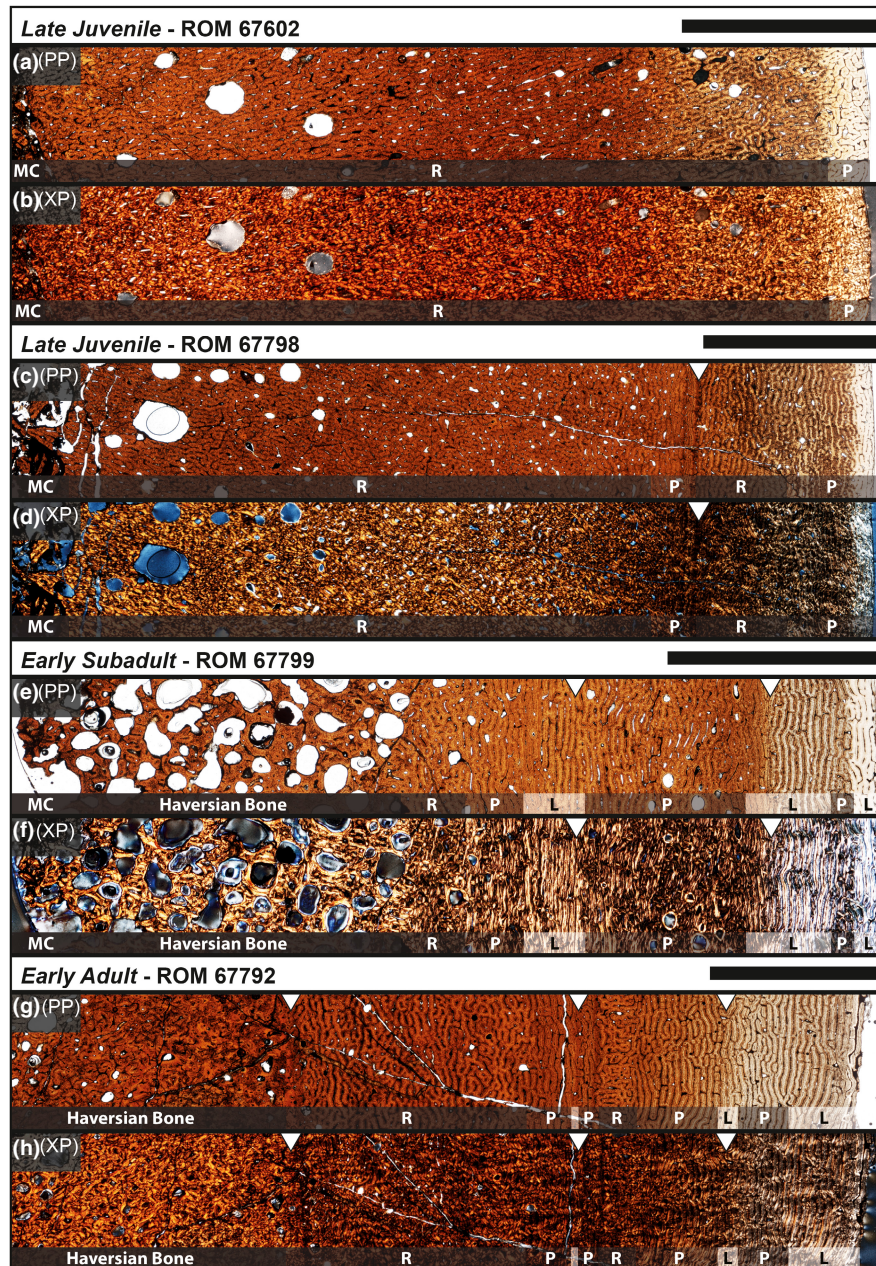
**FIGURE 7** Osteohistology of *Edmontosaurus annectens* humeri from the Ruth Mason dinosaur quarry of South Dakota, United States under plain-polarized (PP) and cross-polarized (XP) light microscopy. (a, b) Late juvenile (ROM 73849). (c, d) Early subadult (ROM 67796). (e, f) Late subadult (ROM 73850). (g, h) Late adult (ROM 67794). Scale bars are 0.5 cm. (l), laminar; MC, medullary cavity; (p), plexiform; R, reticular

#### 4.3.2 | Femur

##### *Late juvenile*

Specimens examined: ROM 67602 (Figure 8a,b), ROM 67798 (Figure 8c,d). After retrodeformation, the mid-diaphyseal perimeter of ROM 67602 had an elliptical shape with a relatively broad minimum axis, whereas ROM 67798 had a more circular shape with rounded corners near the region of the fourth trochanter. The medullary cavities, which constituted ~33% of the entire cross-sectional area in each specimen, reflected the shapes of their respective periosteal perimeters. Because the femora were heavily

distorted from crushing, the medullary cavities of each specimen contained a large central void. However, the preserved portions near the interface between the medullary cavity and the cortical bone distinctly consisted of large erosional cavities transitioning into relatively smaller constituents when moving outwards and into the cortical bone. ROM 67798 best presented this graduated transition, which halted shortly before the single recorded growth mark (226 mm), whereas the smaller erosional cavities continued up to the periosteal surface in ROM 67602; an endosteal margin of the compact bone was not identifiable in either specimen. Much of what was preserved of each medullary cavity and the majority



**FIGURE 8** Osteohistology of *Edmontosaurus annectens* femora from the Ruth Mason dinosaur quarry of South Dakota, United States under plain-polarized (PP) and cross-polarized (XP) light microscopy. (a, b) Late juvenile (ROM 67602). (c, d) Late juvenile (ROM 67798). (e, f) Early subadult (ROM 67799). (g, h) Early adult (ROM 67792). Scale bars are 0.5 cm. L, laminar; MC, medullary cavity; P, plexiform; R, reticular

of the cortical bone was composed of fibrolamellar bone with an underlying woven-fibered matrix organized in a reticular orientation that was overprinted by lamellar bone, particularly around erosional cavities. Parallel-fibered bone comprised the outermost cortex with a transitioning plexiform-laminar vascular canal orientation, as seen in the late juvenile (ROM 73849) and early subadult (ROM 67796) humeri. Because both femora had similar outer circumferences of ~253 mm, we expected them to also have similar growth mark records. However, only ROM 67798 recorded a single growth mark with a similar narrow zone of parallel-fibered/lamellar bone, as in the early subadult humerus (ROM 67796), but

both femora preserved a layering of lamellar bone with laminar vascular canal orientation at the periosteal surface. ROM 67602 presented signs of localized parallel-fibered bone in the region of the ROM 67798 growth mark, but the parallel-fibered bone did not continue around the entire circumference. Secondary osteon development was completely absent throughout each cross section except for the area near the fourth trochanter. Here, secondary osteons with a single cement line were elongated on a diagonal to the perpendicular surface of the nearby periosteal surface and looked as though they were being “pulled” toward the muscle attachment site.

### Early subadult

Specimen examined: ROM 67799 (Figure 8e,f). Similar to the late juvenile femora (ROM 67602; ROM 67798), this specimen had undergone extensive crushing and required retrodeformation. The mid-diaphyseal perimeter and general outline of the medullary cavity were similar to the circular shape of the late juvenile (ROM 67798), but with more defined corners along the anterior side. The medullary cavity constituted 58.9% of the entire cross-sectional area with a very large central void as a result of the crushing. Erosional cavities considerably ranged in size and persisted up until the first growth mark (272 mm) within a substantially remodeled bone matrix that consisted of lamellar bone around the circumference of each erosional cavity. Secondary osteons recorded multiple generations (3+) of cement lines and exhibited exquisite Maltese cross extinction patterns when the cross-polarized filter was rotated. Dense Haversian bone (Reid, 1985) was present along the posterior half of the cross section, particularly in the area of the fourth trochanter, which obscured the growth record in these regions. However, the remainder of the outer cortex of the posterior half and the entire cortical bone of the anterior half of the bone recorded three transitional plexiform-lamellar vascular canal orientation zones separated by two growth marks. Parallel-fibered bone comprised the plexiform oriented portions, whereas the lamellar regions, which included the growth marks, were composed of lamellar bone with interspersed areas of parallel-fibered bone. Prior to the second recorded growth mark (297 mm), the plexiform region exhibited sparsely scattered secondary osteons of varying sizes that continued around the circumference of the cross section, even in areas of dense secondary osteon development. The outermost cortex near the periosteal surface preserved a layering of parallel-fibered/lamellar bone with lamellar vascular canal orientation at the periosteal surface.

### Early adult

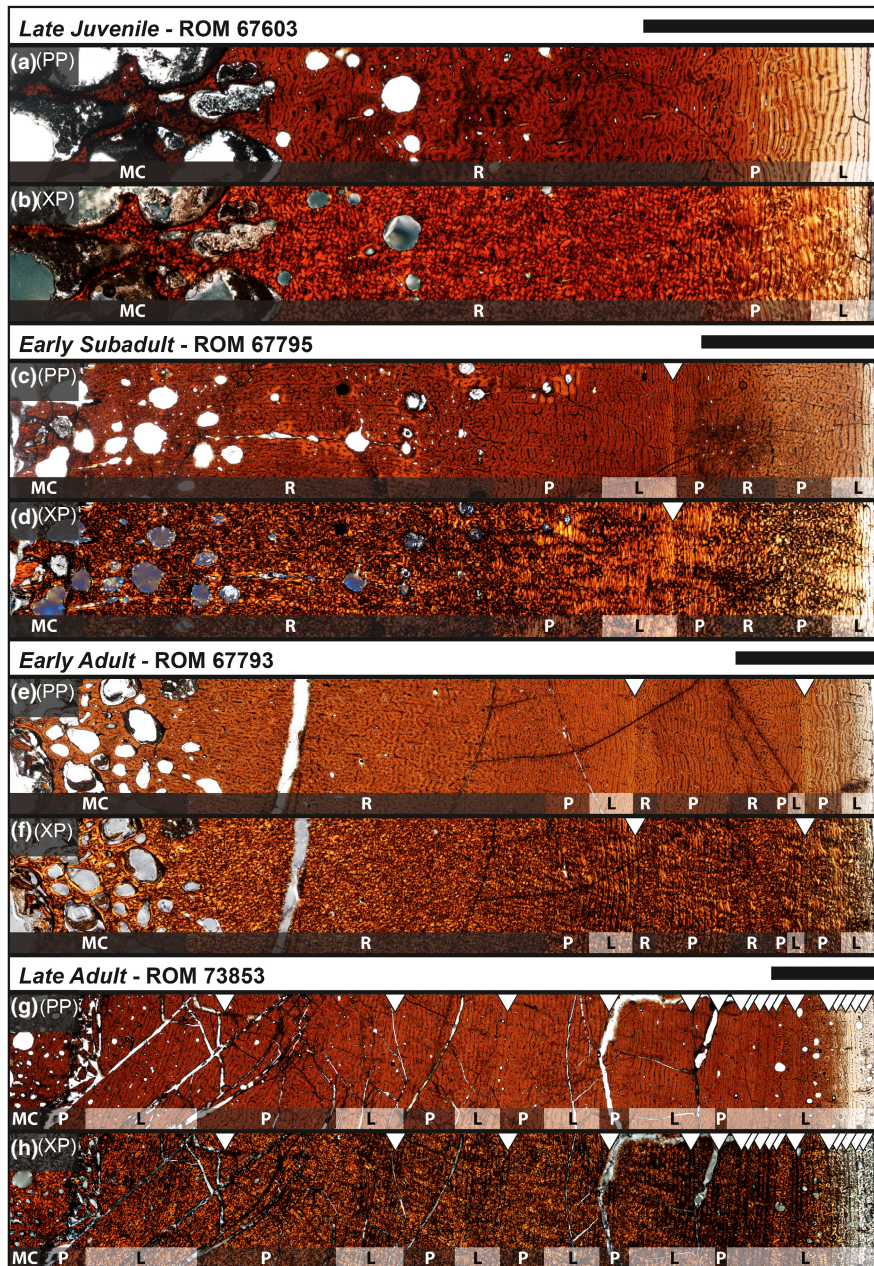
Specimen examined: ROM 67792 (Figure 8g,h). Retrodeformation was again required because of the substantial level of crushing. The mid-diaphyseal perimeter and general outline of the medullary cavity were also circular in shape, but with corners that were more rounded than any of the younger ontogenetic stages. The medullary cavity constituted 67.8% of the entire cross-sectional area with a substantially larger void, resulting in a relatively thin layer of cortical bone. Erosional cavities ranged in size and plentifully persisted up to just before the first growth mark (330 mm), where there were almost no erosional cavities within a parallel-fibered/lamellar bone matrix running parallel with the growth mark. Prior to the first growth mark, any sign of primary bone tissue had been completely obliterated by extremely dense Haversian bone (Reid, 1985). Interestingly, the diameter of the secondary osteons exhibited a substantial reduction when approaching the first growth mark relative to more inner matrix. The zone continuing outwards from the first growth mark was composed of primary parallel-fibered bone with plexiform vascular canal orientation that was interspersed with erosional

cavities; these ranged in size from small along the anterior and lateral sides of the bone to large on the medial and posterior side of the bone, which was closest to the muscle attachment sites and the fourth trochanter. Just prior to the second growth mark (367.5 mm), the orientation of vascular canals shifted from plexiform to lamellar along a narrow layer of lamellar bone. The next zone consisted of a sequence that started with two distinctly narrow bone layers that were present along the circumference of the section; the first was a layer of plexiform oriented parallel-fibered bone, followed by a reticular oriented parallel-fibered layer that was about twice the thickness of the plexiform oriented layer. From the reticular orientation, the vascular canals briefly transitioned through plexiform before arriving at lamellar, all while being composed of lamellar bone. This sequence of transitions is best seen along the anterior side of the specimen. The third growth mark (385 mm) was similar to those in younger individuals where there was no distinct break in bone deposition but rather a substantial reduction. In addition, the second and third growth marks had an opaque color that was consistently present across the entire circumference, even through the heavily remodeled region around the fourth trochanter. The outermost zone was strictly composed of lamellar bone with long lamellar vascular canals and intermittent regions of plexiform orientation. Secondary osteon development was not present in the second, third, and fourth zones, which were adjacent to the third growth mark, except for regions near muscle attachment sites.

### 4.3.3 | Tibia

#### Late juvenile

Specimens examined: ROM 67601, ROM 67603 (Figure 9a,b). After retrodeformation, the mid-diaphyseal perimeters of both cross sections had a circular shape with a rounded corner along the anterolateral side of the bone. This anterolateral corner exhibited a radial strip (Woodward et al., 2015) or anterolateral plug (Hübner, 2012) of radially oriented vascular canals originating from the innermost cortex to the periosteal surface. The external morphology indicated slight scarring similar to other muscle attachment sites, such as those along the fourth trochanter of femora. The medullary cavities, which constituted ~26% of the entire cross-sectional area in each specimen, reflected the shapes of the near-circular periosteal perimeters. The medullary cavity of ROM 67601 was filled in with what perhaps resembled primary trabecular bone that was extremely cancellous, but this could have also been a product of taphonomic deformation. Conversely, the core of the medullary cavity of ROM 67603 did not preserve, and as a result was observed as a voided space. Endosteal margins of the compact bone were not identifiable in either specimen. Moving outwards toward the inner cortex of the bone, large erosional cavities of similar size were present along the circumference at the interface between the medullary cavity and cortical bone. A gradual reduction in size and density of these erosional cavities was observed through the inner



**FIGURE 9** Osteohistology of *Edmontosaurus annectens* tibiae from the Ruth Mason dinosaur quarry of South Dakota, United States under plain-polarized (PP) and cross-polarized (XP) light microscopy. (a, b) Late juvenile (ROM 67603). (c, d) Early subadult (ROM 67795). (e, f) Early adult (ROM 67793). (g, h) Late adult (ROM 73853). Scale bars are 0.5 cm. L, laminar; MC, medullary cavity; P, plexiform; R, reticular

half of the cortical bone and were no longer present in the outer half. A woven-fibered matrix of reticular oriented vascular canals composed the majority of the inner cortex that contained the erosional cavities. The outer cortex exhibited a transition from reticular oriented woven-fibered bone to plexiform oriented parallel-fibered bone with localized regions of laminar orientation near the periosteal surface. Although no complete growth marks were present in either of the two specimens, minor indications of a growth mark just outside of the medullary cavity region were observed in both specimens and estimated roughly at ~100mm. Secondary osteon development was absent in both specimens.

#### Early subadult

Specimens examined: ROM 67795 (Figure 9c,d), ROM 67797. The mid-diaphyseal perimeter of ROM 67795 was very similar to the late juvenile tibiae (ROM 67601; ROM 67603), but with a slightly more pronounced anterolateral corner. The cross-sectional perimeter of ROM 67797 was egg-shaped, even after retrodeformation, with the rounded point being home to the location of the anterolateral plug, suggesting that the section was taken slightly distal of the minimum diaphyseal circumference of the tibia. The medullary cavities, which constituted ~25% of the entire cross-sectional area in each specimen, reflected the shapes of the respective periosteal perimeters.

The anterior side of ROM 67795 had been crushed to the point that much of the cortical bone had caved inwards toward the medullary cavity region and what remained after retrodeformation was sparse and likely misplaced effectively resulting in large voids. Given this, the outline of what was likely the medullary cavity was still recognizable and reflected the periosteal perimeter. The medullary cavity of ROM 67797 did preserve highly vascular trabecular bone along the anteromedial side of the element. Both specimens exhibited the same erosional cavity pattern at the interface between the medullary cavity and cortical bone as observed in the late juveniles (ROM 67601; ROM 67603). The difference was that the pattern diminished just before the growth mark (202 mm) in ROM 67795 but well before in ROM 67797, almost never invading the cortical bone. This dissimilarity could be due to the difference in location of each cross section along the proximal-distal axis of tibial diaphysis. Both medullary cavities were composed of woven-fibered bone with lamellar bone outlining each erosional cavity. Secondary osteons had begun to invade from the medullary cavity with secondary osteons that had as many as four generations of cement lines, but overlap between secondary osteons was not observed. The inner cortex was comprised of fibrolamellar bone with a dense woven-fibered component that was oriented with reticular vascular canals, and occasionally an intermediate stage between radial and reticular. Shortly before the one recorded growth mark in each specimen, the typical transition of reticular to plexiform to lamellar vascular canal orientation was observed. The circumferential region of lamellar orientation just before the growth mark was composed of lamellar bone with a woven-fibered overprint scattered along the circumference. Following the growth mark, the bone transitioned into a narrow zone of parallel-fibered bone oriented with plexiform vascular canals before returning to the distinctive reticular orientation within a fibrolamellar matrix. As with the late juveniles, both early subadults exhibited a layering of parallel-fibered/lamellar bone with lamellar-oriented vascular canals near the periosteal surface.

#### *Early adult*

Specimen examined: ROM 67793 (Figure 9e,f). The mid-diaphyseal perimeter continued the trend of an overall circular shape with a rounded anterolateral corner, which was the only location in the cross-section with radial vascular canal orientation reflecting the characteristics of the anterolateral plug. The medullary cavity, which constituted 23.5% of the entire cross-sectional area, reflected the shape of the near-circular periosteal perimeter. It was partially filled in with cancellous trabecular-like bone composed of a woven-fibered matrix and lamellar bone along the circumference of each erosional cavity. The transition from large to small erosional cavities was quite narrow and was minimally present in the inner cortex up until about the first growth mark (213 mm). The inner cortex was composed of a woven-fibered matrix oriented with reticular vascular canals and went through a very narrow region of plexiform before laying down distinct lamellar oriented parallel-fibered bone leading up to the first growth mark. The next zone went through a sequence starting with reticular oriented woven-fibered bone, followed by a

plexiform oriented woven/parallel-fibered complex, back to reticular oriented woven-fibered bone, before culminating with lamellar oriented parallel-fibered bone. The second growth mark (249 mm) exhibited relatively smaller spacing from the previous zone than the first growth mark and was followed by lamellar to plexiform oriented parallel-fibered bone that transitioned into lamellar near the periosteal surface. Secondary osteon development was minimally present before the first growth mark and not observed in the outer cortex.

#### *Late adult*

Specimens examined: ROM 73852, ROM 73853 (Figure 9g,h). The mid-diaphyseal perimeter of ROM 73852 reflected the overall circular shape and rounded anterolateral corner of smaller size classes. The medullary cavity, which constituted 20.6% of the entire cross-sectional area, was nearly circular and did not extend into the anterolateral corner. It was partially filled in with cancellous trabecular-like bone composed of a woven-fibered matrix and lamellar bone along the circumference of each erosional cavity. Little or no transition from large to small erosional cavities was observed along the circumference of the medullary cavity. Immediately following was a dense inner cortex composed of a woven-fibered matrix with lamellar bone outlining a nominal array of small erosional cavities. This region was beginning to develop extensive secondary remodeling with a concentration of secondary osteons gradually increasing toward the anterolateral corner, which itself exhibited a dense stream of Haversian bone (Reid, 1985) that continued until about the final 0.5 cm of the outer cortex. A total of 12 growth marks were recorded. Those within the inner cortex reflected zonal bone and vascular canal orientation changes similar to juveniles and early subadult individuals. Zones within the outer half of the cortex no longer retained a reticular component and were strictly transitioning between plexiform and lamellar-oriented parallel-fibered bone. The final three growth marks were LAGs and present in the last 0.5 cm of the cortex, which was composed of lamellar bone with some regions along the circumference exhibiting longitudinal vascular canal orientation.

The osteohistology of ROM 73853 was similar in many respects to ROM 73852, but several differences were observed. The anterolateral corner of the outer perimeter was much less prominent giving the overall shape of a cross section near the circular outline. Although secondary osteons were abundantly scattered throughout the entire cortex including the periosteal surface, enough of the primary bone tissue had not yet been obliterated and preserved a growth record of ~18 circumferential growth marks. Secondary osteons were commonly observed lining up alongside the growth marks, some of which are only faintly observed and required the entire cross section for a reconstruction of their circumference. The final six to eight growth marks were LAGs and were present within the last 1 cm of the outer cortex. Two potential instances of double LAGs were observed within the outer layering of growth marks but were tentatively considered as independent growth cycles due to the current lack of understanding surrounding multiple annuli within



individual zones (e.g., Evans et al., 2015; Freedman Fowler & Horner, 2015). In addition, several of these growth marks were only present along the postero-medial half of the cross section and may not have been observed if only a partial cross section or core was taken. The outer layering of LAGs near the periosteal surface potentially resembled the onset of an EFS (Horner et al., 2000) or OCL (Chinsamy-Turan, 2005) and presented an increase in erosional cavities relative to the majority of the cortical bone.

#### 4.4 | Age determination and growth modeling

Data related to parameter values of each growth model for tibia circumference and body mass are available in Tables S2 and S3, respectively. Growth mark circumferences for each sampled specimen are included in Table 1. A summary of estimated body masses for associated skeletons of *Edmontosaurus* is available in Table 2. Tibia circumference and body mass growth curves are presented in Figure 10. From our RMDQ sample, two tibiae preserved a substantial growth record that was suitable for growth modeling.

Retrocalculation was first performed on the individual tibiae, and then the growth records of both individuals were combined to better represent the population. The averaged models indicated that the first recorded growth marks of ROM 73852, ROM 73853, and the combined sample corresponded with 8.19, 4.71, and 4.35 years of age, respectively. These estimates were excessively high and outside of the range of variation relative to other hadrosaurids (Wosik et al., 2020).

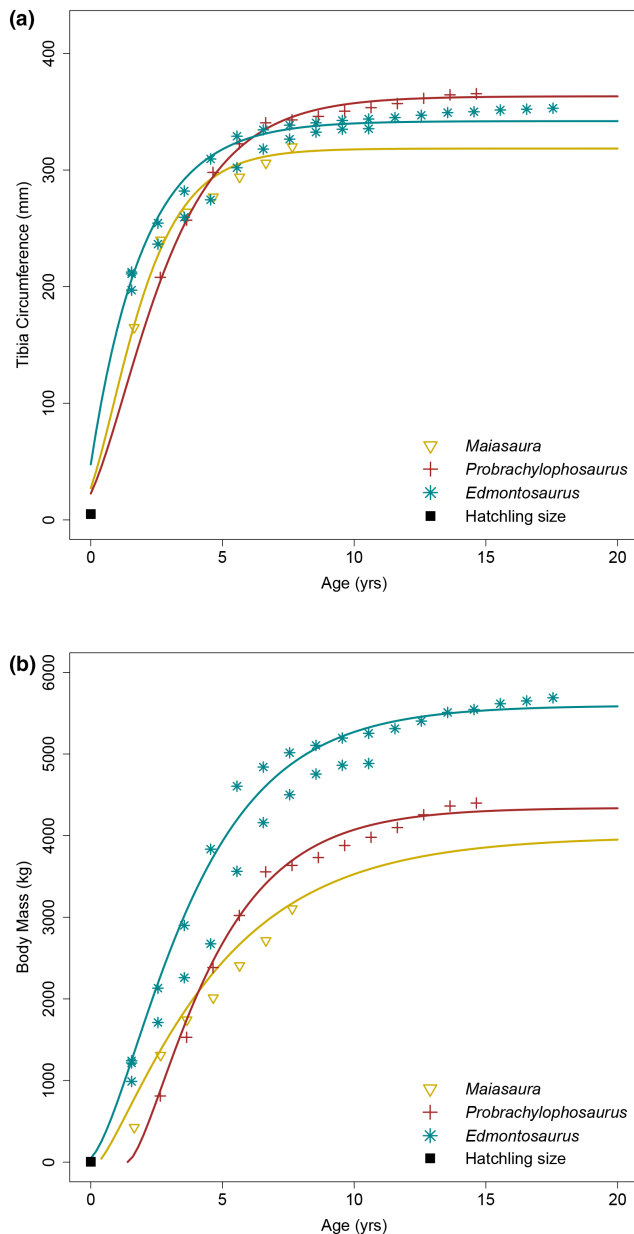
Using the equations produced from the retrocalculation models to estimate the circumferences of the presumably missing growth marks, the histological sections exhibited no signs of growth marks in the prescribed regions, although it might have been possible for the estimated growth marks to have fallen within heavily remodeled areas or within the medullary cavity region. To further investigate the problem, we took the recorded tibial circumference of the yearling growth mark (85 mm) in hadrosaurids from the Dinosaur Park Formation of Alberta, Canada (Wosik et al., 2018; Wosik et al., 2020), and proportionately adjusted it for the larger size of *Edmontosaurus* (Wosik, Goodwin, & Evans, 2017). This indicated that an approximate circumference of 100 mm represented the yearling growth mark of *E. annectens* in the RMDQ sample, and indeed the ~100 mm circumference nested within the outer boundary of the highly remodeled medullary cavity region (Figure 11, MC/SR) of the smallest sampled RMDQ tibiae (ROM 67601; ROM 67603). Retrocalculation on the collective sample, including this hypothetical 100 mm growth mark, indicated that it corresponded with 0.55 years of age, which was better aligned with the osteohistological record presented herein. Therefore, the first recorded growth mark of each individual was determined to correlate with the second year of growth.

The discrepancy could have occurred for a number of reasons. First, the retrocalculation of the growth mark record of *Hypacrosaurus*, as presented in Wosik et al., 2020, was inaccurately estimating the missing age. Through data manipulation (e.g., removing the first recorded growth mark in other individuals), it was determined that more of the growth record at the earlier ontogenetic stages was required to accurately estimate the missing age and could

**TABLE 2** Summary of *Edmontosaurus* body mass estimates of associated skeletons (Wosik, Goodwin, & Evans, 2017) using the intraspecific equation for quadrupedal vertebrates (Campione & Evans, 2012) and development mass extrapolation (DME; Erickson & Tumanova, 2000) using SM R4050 as a presumably adult-sized *E. annectens* individual. % difference is a ratio between the two methods; note juvenile and subadult specimens exhibit the largest discrepancies

Specimen #	Taxon	Femur length	% RMDQ	HC + FC	Body mass (kg)	DME (HC + FC)	% difference
RMDQ max	<i>E. annectens</i>	1233	100.0	740	6075	6102	0.44
AMNH 5730	<i>E. annectens</i>	1147.7	93.1	762.8	6603	6684	1.21
CCM V 1938.8	<i>E. annectens</i>	1152	93.4	776	6922	7037	1.63
CMNH 10178	<i>E. annectens</i>	910	73.8	521	2315	2130	8.71
FPDM	<i>E. annectens</i>	990	80.3	516.5	2261	2075	8.97
LACM 23504	<i>E. annectens</i>	559	45.3	337.5	702	579	21.27
MOR 2939	<i>E. annectens</i>	1175	95.3	782	7070	7201	1.82
SDSM 4917	<i>E. annectens</i>	1032	83.7	617	3685	3537	4.19
SM R4050	<i>E. annectens</i>	-	-	727	5786	5786	0.00
UCMP 137278	<i>E. annectens</i>	995	80.7	621	3752	3606	4.04
USNM 2414	<i>E. annectens</i>	1025	83.1	606	3508	3351	4.68
YPM 2182	<i>E. annectens</i>	1025	83.1	735	5962	5979	0.29
CMN 2289	<i>E. regalis</i>	1242.5	100.8	802	7578	7768	2.44
CMN 8399	<i>E. regalis</i>	1140	92.5	609	3556	3401	4.55
ROM 801 (5167)	<i>E. regalis</i>	1280	103.8	771	6800	6901	1.47

Abbreviation: HC + FC, sum of humerus and femur minimum diaphyseal circumferences.



**FIGURE 10** *Edmontosaurus annectens* growth curves compared with *Maiasaura peeblesorum* and *Probrachylophosaurus bergei*. (a) Tibial minimum diaphyseal circumference growth. (b) Body mass growth



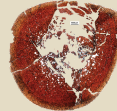

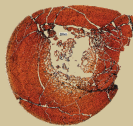
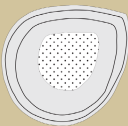
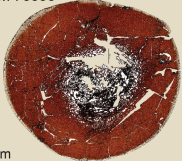
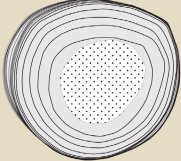
have also been the case here. Second, the hatchling size used was that of hadrosaurids from the Dinosaur Park Formation, which were generally smaller in terms of average adult body size. To test how sensitive the retrocalculated ages were to the hatchling size, the retrocalculation models were rerun using a slightly increased, and hypothetical, hatchling circumference of 35 mm instead of 25 mm. The results indicated a 12% decrease when estimating the missing age and demonstrated that a more accurate hatchling size would likely return more accurate age estimations (Wosik et al., 2018; Wosik, Whitney, et al., 2017). Third, the two late adult tibiae used for growth modeling may have reflected substantially different growth strategies, indicating a high level of variation within the population.

The combined population containing the hypothetical 100 mm growth mark was analyzed using the respective retrocalculated ages. Growth began to slow down after age six and 95% body mass was attained by about age nine. The growth trajectory between the two tibiae revealed a small degree of variation; therefore, the presented growth curve was intended to be an average of the two individuals. The transition from growth acceleration to deceleration, or the growth inflection point, occurred at 1.67 years of age, which was similar to values of 1.40 years of age for that of *Maiasaura* (Wosik et al., 2020 reanalysis of Woodward et al., 2015). The shape parameter  $m$  of the *Edmontosaurus* growth curve resembled an intermediate between the monomolecular and von Bertalanffy models ( $m = 0.48$ ). The average asymptotic body mass of *E. annectens* individuals from the RMDQ was ~5595 kg.

## 5 | DISCUSSION

This study represents one of the most thorough attempts to assess growth and demography in an extinct dinosaur using a comprehensive integration of size-frequency distributions and long bone histology. Late juvenile individuals of *Edmontosaurus annectens* from the Ruth Mason Dinosaur Quarry (RMDQ), South Dakota, all had primary bone tissues exhibiting a large medullary cavity surrounded by highly vascularized, woven-fibered bone within the inner cortex, indicating rapid growth. The vascularity of the outer cortex largely consisted of zonal bone, transitioning from reticular/plexiform into laminar, demonstrating a cyclical growth pattern. Sub-adults retained the highly vascularized, woven-fibered inner cortex. Prominent lines of arrested growth (LAGs) appeared in the outer cortex of only the most mature individuals (ROM 67794; ROM 73852; ROM 73853). However, nearly all individuals, except for a few of the late juveniles, exhibited growth marks comprised of a narrow but gradational shift from laminar to reticular oriented vascular canals similarly observed in *Maiasaura* (Woodward et al., 2015). Adults, represented by the largest bones in the sample, had well developed secondary osteons, and the non-zonal outermost cortex was comprised solely of laminar oriented vascular canals in lamellar bone, indicating the onset of skeletal maturity. Pronounced stacking of LAGs is preserved, indicating the adult individuals (ROM 67794; ROM 73852; ROM 73853) were approaching asymptotic body size. Late juveniles and sub-adults exhibited a stronger zonation of bone with consistent, repeated shifts between reticular and laminar oriented fibrolamellar bone than was seen in adults. All sectioned elements showed a layering of laminar oriented parallel-fibered or lamellar bone near the periosteal surface that likely signaled the imminent formation of a growth mark.

When integrating the osteohistological data with that from the size-frequency distributions, growth marks were generally offset from and occasionally larger than the outer circumferences (periosteal surfaces) of individuals belonging to the size-frequency peak of the corresponding size-class (Figure 3b). However, there was a consistent correlation between individual size-frequency peaks and clusters of growth marks, indicating that the size-frequency peaks

Size Class	Histology	Schematic	Circumferences (mm)		
			MC/SR	GM 1	Outer
Late Juvenile	ROM 67603 		98	(100)	185
Early Subadult	ROM 67795 		121	202	238
Early Adult	ROM 67793 		130	213	267
Late Adult	ROM 73853 		173	212	355

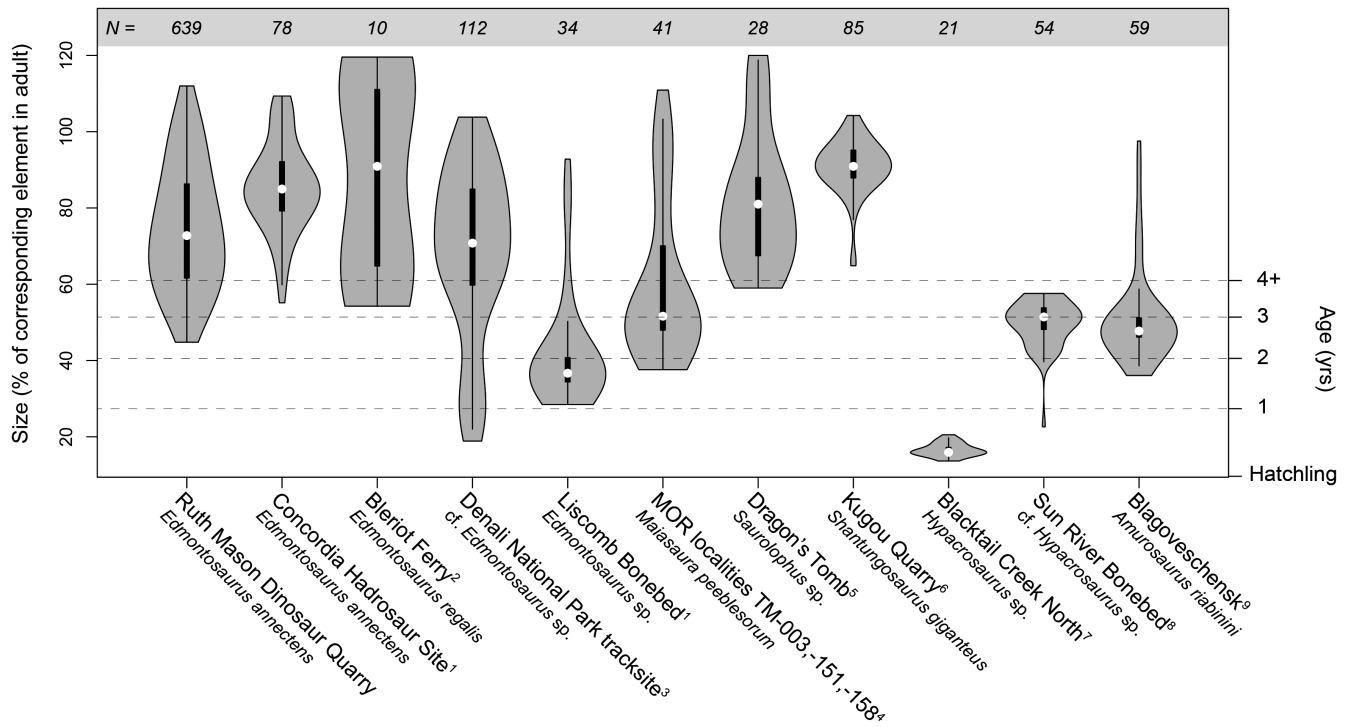
**FIGURE 11** Summary of section stacking of tibiae demonstrating the obliteration of the inner cortex (early ontogeny) via processes of secondary bone remodeling. Schematics highlight cortical bone (solid gray), extent of medullary cavity and/or secondary osteon development (dotted white), and growth marks (solid black line). Circumferences refer to the extent of the medullary cavity and/or extensive inner cortex secondary remodeling (MC/SR), growth mark (GM), and outer/periosteal circumference (outer). The imaged thin sections were retrodeformed, except for ROM 67793 for which most of the periosteal margin and cortical bone remained intact

in the size-frequency distributions were likely representing cohorts, which is consistent with the taphonomic interpretation of catastrophic assemblages (e.g., Olson, 1957; Voorhies, 1969). This pattern was prevalent early in ontogeny up until the late subadult stage, or third size-frequency peak, when age ranges based on growth marks began to overlap. A similar pattern was observed in the attritional assemblage of hadrosaurids from the Dinosaur Park Formation of Alberta, Canada (Wosik et al., 2020). Individuals sampled from the first size-frequency peak either recorded one growth mark or exhibited a distinct layering of laminar vascular canals near the periosteal surface, suggesting the imminent formation of a growth mark; this annulus was approximately the size of the first recorded growth mark in older individuals of the same element.

Integrating these data with the growth modeling results, we determined that the first size-frequency peak (late juveniles) most likely corresponds with 2-year-old individuals (Figure 3). By this stage, the medullary cavity had already expanded beyond the circumference of the estimated yearling growth mark of ~100mm (Figure 11). In fact, the RMDQ sample did not contain individuals smaller than about 40% of asymptotic adult body size for *E. annectens* (Figure 12). Although smaller sized individuals can be subject to hydraulic sorting (Brown, Evans, Ryan, & Russell, 2013; Brown, Evans, Campione, et al., 2013), the results of the RMDQ autopodial

element size-frequency distribution (Figure 6) indicated that autopodial elements were present in excess and did not vary in their overall degree of completeness relative to long bones from the same population. This suggests that taphonomic biases had not contributed toward the absence of nestling-sized long bones in the RMDQ sample, which were hydraulically equivalent to late juvenile-adult autopodial elements, providing further evidence that segregation between nestling-juvenile and adult hadrosaurids may have been a real biological signal (e.g., Holland et al., 2021; Lauters et al., 2008; Varricchio & Horner, 1993; Wosik et al., 2020).

Individuals from the second size-frequency peak (early subadults) recorded two growth marks in addition to the outer laminar layering and corresponded with 3-year-old individuals. The third size-frequency peak (late subadults) had growth mark age ranges that overlapped between 4- and 5-year-old individuals. By this stage, the degree of secondary remodeling, particularly the expansion of the medullary cavity and development of secondary osteons, had already obliterated the 2-year-old growth mark in the samples of humeri and femora. This pattern continued in subsequent size-frequency peaks for both of these elements, whereas the tibiae recorded all of the preceding growth marks, except for the estimated yearling growth mark, in each specimen regardless of ontogenetic stage (Figure 11), corroborating that tibiae provide the most consistently complete



**FIGURE 12** Density comparison of long bone and tracksite size distributions of hadrosaurid bonebeds. N refers to sample size. Data for temperate and polar populations were derived from published literature: <sup>1</sup>This study; <sup>2</sup>Evans et al. (2015); <sup>3</sup>Fiorillo et al. (2014); <sup>4</sup>Woodward et al. (2015); <sup>5</sup>Bell et al. (2018); <sup>6</sup>Hone et al. (2014); <sup>7</sup>Varricchio and Horner (1993); <sup>8</sup>Scherzer and Varricchio (2010); <sup>9</sup>Lauters et al. (2008)

growth record (Horner et al., 1999; Woodward et al., 2015). The fourth size-frequency peak (early adults) consisted of individuals 5–7 years of age, and the final fifth size-frequency peak consisted of late adults 6 years of age and older, with one individual approaching 20 years (ROM 73853). Although the three most mature individuals from the sample fell within the late adult size class, the inclusive adult size class of RMDQ demonstrates that there was a certain degree of variation in the growth and asymptotic body size within a single *E. annectens* population. Therefore, the use of size-frequency peaks, or size-classes, from size-frequency distributions can only be used as a proxy for age in early ontogeny and requires the integration of osteohistological data to accurately identify the precise ontogenetic age of each size class, which is consistent with the results from a similarly sampled attritional assemblage of hadrosaurids from the Dinosaur Park Formation (Wosik et al., 2020).

The body mass growth curve analysis of the RMDQ *E. annectens* sample indicated that the average asymptotic body mass was ~5595 kg, whereas the maximum was ~6075 kg and was calculated using the minimum diaphyseal circumferences from the largest RMDQ humerus and femur and the well-established interspecific body mass equation for quadrupedal vertebrates (Campione & Evans, 2012). When comparing the maximum RMDQ body mass with estimated body masses of associated skeletons of *Edmontosaurus* (Table 2), RMDQ maximum size ranked among the highest and just under AMNH 5730 (~6603 kg) and CCM V 1938.8 (~6922 kg), both of which were initially referred to *Anatotitan* (sensu Brett-Surman, 1989), but have since been empirically synonymized as the ontogenetic end members of *E. annectens* by Campione and Evans (2011). The late juvenile LACM 23504 was estimated to be

~579 kg based on DME (Erickson & Tumanova, 2000), and because it consistently placed within the late juvenile size class of RMDQ (Figure 5), it provided an approximate lower bound estimate for the RMDQ population and an approximate body mass for individuals approaching 2 years of age. Interestingly, the holotype of *E. annectens*, USNM 2414 (Marsh, 1892), placed within the early adult size class (Figure 3A) and had an estimated body mass of ~3351 kg, suggesting that it had not yet attained skeletal maturity; this will be the focus of an additional study. When compared with other hadrosaurids, the average asymptotic body mass (~5595 kg) of *E. annectens* individuals from the RMDQ was ~257 kg greater than the body mass of the largest hadrosaurid individual from the Dinosaur Park Formation (TMP 1979.014.0020, 5338 kg) and was approximately 1250–1600 kg greater than hadrosaurids from the Two Medicine Formation of Montana (*Probrachylophosaurus*, *Maiasaura*, and *Hypacrosaurus*; Wosik et al., 2020). Despite these differences, *E. annectens* had attained 95% of its asymptotic body mass by about 9 years of age, which is similar to estimates of 9 years for *Maiasaura* and *Probrachylophosaurus* (Wosik et al., 2020) and 7 years for individuals from the DPF (Wosik et al., 2020). Given this, we hypothesize that hadrosaurids inherited a similar growth strategy attaining asymptotic body size between seven and nine years of age.

## 5.1 | Population dynamics of *Edmontosaurus*

Hadrosaurid dinosaurs have been historically defined as being gregarious based on evidence of numerous bonebed accumulations (e.g., Christians, 1992; Colson et al., 2004; Horner et al., 2004; Lauters

et al., 2008; Scherzer & Varricchio, 2010; Bell & Campione, 2014; Eberth et al., 2014; Hone et al., 2014; Evans et al., 2015; Woodward et al., 2015; Ullmann et al., 2017; Bell et al., 2018; Holland et al., 2021). However, before estimating the population dynamics of an extinct animal, the depositional origin of the sampled assemblage, including the manner of death, need to be assessed. If an assemblage is attritional, or selective, it preserves a time-averaged and potentially biased sample of mortality of a hypothetical population over time in a given area, whereas a catastrophic, or non-selective, assemblage provides a snapshot of the standing crop as it existed at one time (Olson, 1957; Voorhies, 1969). Only a catastrophic assemblage will presumably provide data on the proportions of individuals and cohorts within a living population, but in most cases, a bonebed will become secondarily altered (e.g., winnowing, scavenging, disarticulation, overprinting), making it more difficult to identify the depositional origin (Rogers & Kidwell, 2007) and may subsequently influence interpretations related to population structure. Therefore, it is important to present data beyond geological and taphonomic information to determine the accurate depositional nature of the assemblage.

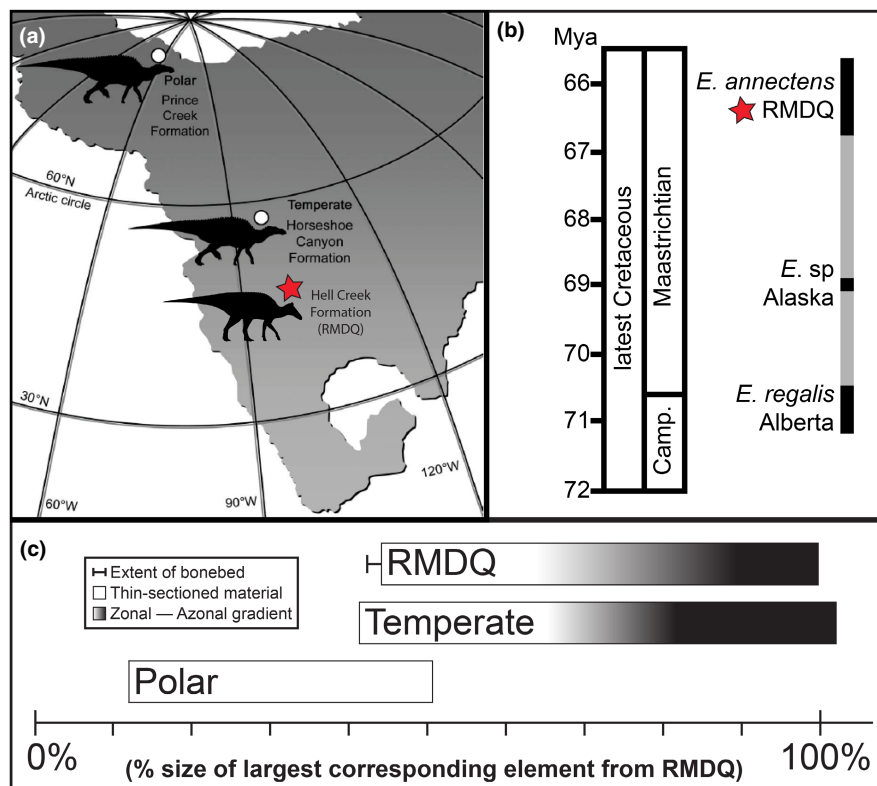
Based on data from a previous geological and taphonomic study of the RMDQ (Christians, 1992), this *E. annectens* bonebed has been defined as a catastrophic assemblage that was secondarily deposited locally. Our data provide further evidence on the manner of death of this assemblage. When size-frequency distributions from individual elements were consolidated into a combined size-frequency distribution, size-frequency peaks aligned not only between different elements, but also with the osteohistologically determined ages, suggesting that cohorts constituted the size-frequency peaks. The proportions of these cohorts reflected the general distributions of catastrophic assemblages in that each subsequent cohort consisted of fewer individuals than the previous cohort, resulting in a step-wise reduction toward somatically mature adults (Olson, 1957). The external morphology and minimal signs of abrasion supported previous conclusions that any secondary transport was minimal. The entire sample of osteohistologically sectioned individuals preserved a similar layering of laminar vascular canals, suggesting that the mass death event was tied to a single season that correlated with the slow-growing period. This collective integration of morphological, osteohistological, geological, and taphonomic data for RMDQ provides exceptionally strong evidence of a monodominant catastrophic bonebed of a hadrosaurid population.

Size-frequency profiles of RMDQ allow the population dynamics of *E. annectens* to be understood more completely. Because of its catastrophic genesis, cohorts were presumably preserved proportionately to the standing crop of the living population. Given this, we can confidently infer that *E. annectens* individuals congregated into large herds for a portion of the year that at least corresponded with the slow-growing season. The composition of herds ranged from 2-year-old late juveniles (~1200 kg) to mature adults (>5000 kg) of at least 18 years of age (ROM 73853), suggesting that somatically mature adults likely remained within the herd until death. When compared with other *Edmontosaurus* bonebeds (Figure 12),

the absence of nestling- and yearling-sized individuals further supports the hypothesis of segregation from older cohorts (e.g., Varricchio & Horner, 1993; Lauters et al., 2008; Wosik et al., 2020). Interestingly, this is further supported by the size profile of the Liscomb *Edmontosaurus* Bonebed from the Prince Creek Formation of the North Slope of Alaska (Gangloff & Fiorillo, 2010). With the exception of a partially preserved and potentially misidentified adult tibia (personal communication with A. Fiorillo and R. Takasaki), the Liscomb Bonebed consists of yearling to 2-year-old individuals that would bridge the gap between nestlings (Wosik, Goodwin, & Evans, 2017; Wosik et al., 2019) and the RMDQ population. If these estimated ages are accurate, this suggests that late-nestling to juvenile individuals formed their own potentially independent groups, and these individuals reintegrated with the main herd between 2 and 3 years of age. Juvenile groups have been noted in other iguanodontian taxa as well (Forster, 1990), including lambeosaurines (Scherzer & Varricchio, 2010; Holland et al., 2021).

## 5.2 | Reevaluating the effects of environmental stressors on osteohistology in *Edmontosaurus*

Previous comparative osteohistological analyses of polar and temperate populations of *Edmontosaurus* from the Maastrichtian (Late Cretaceous) of North America have suggested that polar populations overwintered in their resident polar paleoenvironment rather than migrating to less harsh regions (Chinsamy et al., 2012). Long bones of *Edmontosaurus* sp. from the Prince Creek Formation of Alaska (Gangloff & Fiorillo, 2010), which were derived from small individuals under 2 years of age, showed textural shifts between reticular and laminar (circumferential) fibrolamellar bone vascularization (Chinsamy et al., 2012). Conversely, long bones from a sample of larger *E. regalis* from the Horseshoe Canyon Formation of southern Alberta contained individuals that inconsistently exhibited these textural switches (Chinsamy et al., 2012). The authors suggested that textural shifts resulted from environmental stressors, not migratory behavior, and proposed that all individuals in the polar population showed textural shifts because they were subjected to very strong environmental stressors in the form of harsh winters (Chinsamy et al., 2012), when not only temperature but sunlight and related changes in forage quality and availability would be detrimental to growth and survival. Only some individuals in the temperate population showed textural shifts because the environment was interpreted to have been more stable, with only occasional decreases in winter forage quality that did not uniformly affect each individual (see also Vandervan et al., 2014). Therefore, variability in bone histology within and between *Edmontosaurus* populations was interpreted to reflect the intensity of environmental stressors, not movement away from such stressors. Although this is an interesting hypothesis, evaluating it is confounded by the differently sized individuals, of potentially different ontogenetic stages, that were sampled from the polar (juvenile) and temperate (subadult-adult) populations (Figure 13c).



**FIGURE 13** (a) Polar and temperate localities of *Edmontosaurus* (modified from Chinsamy et al., 2012). (b) biostratigraphy of *Edmontosaurus* (modified from Campione & Evans, 2011). (c) schematic of zonal-azonal bone across ontogenetic stages. Data for polar and temperate derived from Chinsamy et al., 2012

The latitudinal differences in multiple congeneric *Edmontosaurus* bonebeds (Figure 13A) provide a rare study sample to investigate whether these osteohistological differences are indeed related to environmental stressors, or due to the sampling of differently sized individuals of potentially different ontogenetic stages (Nelms, 1989; Fiorillo & Gangloff, 2001; Campione & Evans, 2011). Relative to the size of the RMDQ population (Figure 13c), the polar population consists primarily of juvenile-sized individuals, with a maximum body size of ~51% of the largest corresponding element from RMDQ. The corresponding RMDQ individuals were still undergoing rapid growth of primary bone tissues subject to little, if any, secondary osteon development. The RMDQ and temperate populations had similar size ranges of late juveniles to late adults. The largest individuals in the RMDQ sample (ROM 67794; ROM 73853) exhibit substantial secondary osteon development, which obscures large portions of their individual growth records. When reviewing the material from the temperate population, femora UALVP 52731 and 47920 (Chinsamy et al., 2012: Figure 3a,b) were greater than 1150mm in total length and preserved only one cycle or lacked any zonal bone, respectively, of reticular-laminar (laminar is referred to as circumferential in Chinsamy et al., 2012) oriented fibrolamellar bone. This was because they exhibited substantial secondary osteon development that had obliterated the primary bone tissue and the original growth record, characteristics indicative of late adults. The third example, UALVP 52696 (Chinsamy et al., 2012: Figure 3c) recorded three zonal shifts because it was a subadult and was still undergoing

rapid growth. Therefore, rather than distinguishing between migration and overwintering, our study indicates that the putative differences between the temperate and polar populations more likely reflect the growth stages of the individuals in each sample. Further studies should explicitly focus on comparing overlapping material over a range of size and age classes to test for latitudinal differences in dinosaurian growth strategies. It is also important to note that the large tibia from the polar population (DMNH 22557; Chinsamy et al., 2012: Figure 2a), which recorded about eight growth cycles, may have been initially misidentified in the collection database (personal communication A. Fiorillo and R. Takasaki) because it was not part of the Liscomb Bonebed assemblage and its fragmentary preservation of only a partial diaphysis makes taxonomic identification ambiguous. If this putative adult specimen, which resembles patterns of vascularity as observed in early adults from the RMDQ, is removed from the polar population dataset, the size distribution of the polar assemblage would not exceed 50% of the largest individuals from the RMDQ. As a result, ontogenetic overlap of the polar vs. temperate/RMDQ assemblages would not exist, voiding any comparison. Based on our observations of the distribution of well-developed zonal bone in similar-sized juveniles of *E. annectens*, we interpret the observed zonal pattern of bone deposition in the polar sample as the result of its juvenile nature rather than arctic seasonality. In addition, studies on modern large-bodied herbivores (Köhler et al., 2012; Mumby et al., 2015) have revealed that physiology drives seasonal growth cycles within the bone microstructure,

suggesting that external environmental stressors may only have a secondary and indirect influence.

## 6 | CONCLUSION

This study analyzed growth and demography in a large sample of the hadrosaurid dinosaur *E. annectens* derived from a monodominant bonebed interpreted as a catastrophic death assemblage. When the size-frequency and osteohistological datasets were combined, growth marks aligned with size-frequency peaks, with the exclusion of the overlapping subadult-adult size range, indicating a strong size-age relationship in early ontogeny. A growth curve analysis of the tibia indicated that *E. annectens* exhibited a similar growth trajectory to other hadrosaurids, suggesting that the clade inherited and utilized a similar growth strategy. Individuals smaller than 40% of the largest corresponding element from this population were not present in this catastrophic assemblage, providing further support that juvenile hadrosaurids were segregated from adults. Osteohistological comparison with material from polar and temperate populations of *Edmontosaurus* revealed that previous conclusions linking osteohistological growth patterns with the strength of environmental stressors were a result of sampling non-overlapping ontogenetic growth stages, with the observed zonal pattern of bone deposition in the polar sample likely the result of its juvenile nature.

## ACKNOWLEDGMENTS

Access to specimens was facilitated by P. Larson and B. Ferrar (BHIGR), N. Carroll (CCM), C. Boyd, J. Persons, and B. Barnes (NDGS), K. Seymour and B. Iwama (ROM), W. Ripley and D. Evans (TCM), and C. Eaton and D. Lovelace (UWGM). This study would not have been possible without taphonomic and field data provided by P. Larson, to whom we are grateful. Funding for this project was generously provided by a Dinosaur Research Institute Student Project Grant (to MW), a Joseph Bazylewicz Fellowship (to MW), a University of Toronto Fellowship (to MW), and a National Sciences and Engineering Research Council Discovery Grant (to DCE; NSERC Grant File Number: RGPIN-2018-06788). Life reconstructions and silhouettes were prepared by D. Dufault (ROM). Preparation of specimens was assisted by S. Sugimoto (ROM), I. MacDonald (TMP), I. Morrison (ROM), and L. Yeider. Wiresaw access for cutting of large specimens was granted by K. Tait (ROM) and facilitated by I. Nicklin (ROM). Discussions with C. Brown, K. Chiba, A. Chinsamy-Turan, M. Laflamme, D. McLennan, R. Reisz, M. Ryan, M. Silcox, D. Tanke, C. Woodruff, and H. Woodward greatly enhanced this manuscript. We thank P. Cox, E. Fenton, H. Xing, and an anonymous reviewer for their helpful suggestions during review. We also thank K. Binner for copy-editing the manuscript prior to initial submission.

## AUTHORS' CONTRIBUTIONS

Mateusz Wosik and David C. Evans designed the study and acquired and analyzed the data. The first draft of the manuscript was prepared by Mateusz Wosik, which then received input from David C. Evans.

## DATA AVAILABILITY STATEMENT

All data that support findings generated during this study are available from the corresponding author upon request.

## ORCID

Mateusz Wosik  <https://orcid.org/0000-0002-0438-5177>

## REFERENCES

- Barretto, C. (1997) Dinosaur growth plates and dinosaur bone growth. In: Wolberd, D.L., Stump, E. & Rosenberg, G.D. (Eds.) *Dinofest International: Proceedings of a symposium held at Arizona State University*. Tempe, AZ: The Academy of Natural Sciences, pp. 95–100.
- Bartoń, K. (2017) Multi-model inference. 1.40.0 ed CRAN.
- Behrensmeier, A.K. (1978) Taphonomic and ecologic information from bone weathering. *Paleobiology*, 4(2), 150–162.
- Bell, P.R. & Campione, N.E. (2014) Taphonomy of the Danek bonebed: a monodominant *Edmontosaurus* (Hadrosauridae) bonebeds from the horseshoe canyon formation, Alberta. *Canadian Journal of Earth Sciences*, 51(11), 992–1006. <https://doi.org/10.1139/cjes-2014-0062>
- Bell, P.R., Evans, D.C., Eberth, D.A., Fanti, F., Tsogtbaatar, K. & Ryan, M.J. (2018) Sedimentological and taphonomic observations on the “Dragon's tomb” *Saurolophus* (Hadrosauridae) bonebed, Nemegt formation (upper cretaceous) Mongolia. *Palaeogeography Palaeoclimatology Palaeoecology*, 494, 75–90. <https://doi.org/10.1016/j.palaeo.2017.11.34>
- Brett-Surman, M.K. (1989). *A revision of the Hadrosauridae (Reptilia: Ornithischia) and their evolution during the Campanian and Maastrichtian*. Ph.D. thesis, George Washington University, Washington, D.C.
- Brinkman, D.B. (2014) The size-frequency distribution of hadrosaurs from the Dinosaur Park formation of Alberta, Canada. In: Eberth, D.A. & Evans, D.C. (Eds.) *Hadrosaurs*. Bloomington, IN: Indiana University Press, pp. 416–421.
- Brown, C.M., Evans, D.C., Campione, N.E., O'Brien, L.J. & Eberth, D.A. (2013) Evidence for taphonomic size bias in the Dinosaur Park formation (Campanian, Alberta), a model Mesozoic terrestrial alluvial-paralic system. *Palaeogeography, Palaeoclimatology, Palaeoecology*, 372, 108–122. <https://doi.org/10.1016/j.palaeo.2021.06.027>
- Brown, C.M., Evans, D.C., Ryan, M.J. & A.P. Russell (2013). New data on the diversity and abundance of small-bodied ornithopods (Dinosauria: Ornithischia) from the Belly River group (Campanian) of Alberta. *Journal of Vertebrate Paleontology*, 33(3), 495–520. <https://doi.org/10.1080/02724634.2013.746229>
- Buffrenil, V. & Castanet, J. (2000) Age estimation by skeletochronology in the Nile monitor (*Varanus niloticus*), a highly exploited species. *Journal of Herpetology*, 34(3), 414–424. <https://doi.org/10.2307/1565365>
- Buffrenil, V., de Ricqlès, A.J., Zylberberg, L. & Padian, K. (2021) *Vertebrate skeletal histology and paleohistology*. Boca Raton, FL: CRC Press, pp. 1–838.
- Burnham, K.P. & Anderson, D.R. (2002) *Model selection and multimodel inference: a practical information-theoretic approach*. New York, NY: Springer-Verlag New York, pp. 1–488.
- Bybee, P.J., Lee, A.H. & Lamm, E.-T. (2006) Sizing the Jurassic theropod dinosaur *allosaurus*: assessing growth strategy and evolution of ontogenetic scaling of limbs. *Journal of Morphology*, 267(3), 347–259. <https://doi.org/10.1002/jmor.10406>
- Campione, N.E. & Evans, D.C. (2011) Cranial growth and variation in edmontosaurs (Dinosauria: Hadrosauridae): implications for latest cretaceous megaherbivore diversity in North America. *PLoS ONE*, 6(9), e25186. <https://doi.org/10.1371/journal.pone.0025186>
- Campione, N.E. & Evans, D.C. (2012) A universal scaling relationship between body mass and proximal limb bone dimensions in quadrupedal terrestrial tetrapods. *BMC Biology*, 10(1), 60. <https://doi.org/10.1186/1741-7007-10-60>

- Chiba, K. (2018). *Osteohistological reconstruction of body mass growth curves and extinct tetrapods*. Ph.D. thesis, University of Toronto. Toronto: University of Toronto.
- Chiba, K., Evans, D.C. & Ryan, M.J. (2015) Assessment of age retrocalulation methods in dinosaur growth studies: a case study using the centrosaurine ceratopsid *Centrosaurus apertus* (Campanian). *Journal of Vertebrate Paleontology*, Program and Abstracts, 106.
- Chinsamy, A. (1993) Bone histology and growth trajectory of the prosauropod dinosaur *Massospondylus carinatus* Owen. *Modern Geology*, 18(3), 319–329.
- Chinsamy-Turan, A. (2005) *The microstructure of dinosaur bone: Deciphering biology with fin-scale techniques*. Baltimore and London: The Johns Hopkins University Press, pp. 1–195.
- Chinsamy, A., Thomas, D.B., Tumarkin-Deratzian, A.R. & Fiorillo, A.R. (2012) Hadrosaurs were perennial polar residents. *The Anatomical Record*, 295(4), 610–614. <https://doi.org/10.1002/ar.22428>
- Christians, J.P. (1992). *Taphonomy and sedimentology of the Mason dinosaur quarry, Hell Creek formation (upper cretaceous), South Dakota*. M.Sc. thesis, University of Wisconsin, Madison.
- Colson, M.C., Colson, R.O. & Nellermeoe, R. (2004) Stratigraphy and depositional environments of the upper Fox Hills and lower Hell Creek formations at the Concordia hadrosaur site in northwestern South Dakota. *Rocky Mountain Geology*, 39(2), 93–111. <https://doi.org/10.2113/39.2.93>
- Cooper, L.N., Lee, A.H., Taper, M.L. & Horner, J.R. (2008) Relative growth rates of predator and prey dinosaurs reflect effects of predation. *Proceedings of the Royal Society London B*, 275(1651), 2609–2615. <https://doi.org/10.1098/rspb.2008.0912>
- Dilkes, D.W. (2000) Appendicular myology of the hadrosaurian dinosaur *Maiasaura peeblesorum* from the late cretaceous (Campanian) of Montana. *Transactions of the Royal Society of Edinburgh: Earth Sciences*, 90(2), 87–125.
- Dilkes, D.W. (2001) An ontogenetic perspective on locomotion in the late cretaceous dinosaur *Maiasaura peeblesorum* (Ornithischia: Hadrosauridae). *Canadian Journal of Earth Sciences*, 38(8), 1205–1227. <https://doi.org/10.1139/cjes-38-8-1205>
- Eberth, D.A., Evans, D.C. & Lloyd, D.W.H. (2014) Occurrence and taphonomy of the first documented hadrosaurid bonebed from the Dinosaur Park Formation (Belly River Group, Campanian) at Dinosaur Provincial Park, Alberta, Canada. In: Eberth, D.A. & Evans, D.C. (Eds.) *Hadrosaurs*. Bloomington: Indiana University Press, pp. 502–523.
- Erickson, G.M., Currie, P.J., Inouye, B.D. & Winn, A.A. (2006) Tyrannosaur life tables: an example of nonavian dinosaur population biology. *Science*, 313(5784), 213–217. <https://doi.org/10.1126/science.1125721>
- Erickson, G.M., Curry Rogers, K. & Yerby, S.A. (2001) Dinosaurian growth patterns and rapid avian growth rates. *Nature*, 412(6845), 429–433. <https://doi.org/10.1038/35086558>
- Erickson, G.M. & Tumanova, T.A. (2000) Growth curve of *Psittacosaurus mongoliensis* Osborn (Ceratopsia: Psittacosauridae) inferred from long bone histology. *Zoological Journal of the Linnean Society*, 130(4), 551–566. <https://doi.org/10.1111/j.1096-3642.2000.tb02201.x>
- Evans, D.C., Eberth, D.A. & Ryan, M.J. (2015) Hadrosaurid (*Edmontosaurus*) bonebeds from the horseshoe canyon formation (Horseshoe member) at Drumheller, Alberta, Canada: geology, preliminary taphonomy, and significance. *Canadian Journal of Earth Sciences*, 52(8), 642–654. <https://doi.org/10.1139/cjes-2014-0184>
- Farke, A. & Yip, E. (2019) A juvenile cf. *Edmontosaurus annectens* (Ornithischia, Hadrosauridae) femur documents a poorly represented growth stage for this taxon. *Vertebrate Anatomy Morphology Palaeontology*, 7. <https://doi.org/10.18435/vamp29347>
- Fiorillo, A.R. & Gangloff, R.A. (2001) The caribou migration model for Arctic hadrosaurs (Dinosauria: Ornithischia): a reassessment. *Historical Biology*, 15(4), 323–334. <https://doi.org/10.1080/0891296021000037327>
- Fiorillo, A.R., Hasiotis, S.T. & Kobayashi, Y. (2014) Herd structure in late cretaceous polar dinosaurs: a remarkable new dinosaur tracksite, Denali National Park, Alaska, USA. *Geology*, 42(8), 719–722. <https://doi.org/10.1130/G35740.1>
- Forster, C.A. (1990) Evidence for juvenile groups in the ornithomimid dinosaur *Tenontosaurus tilletti*, Ostrom. *Journal of Paleontology*, 64(1), 164–165.
- Francillon-Vieillot, H., de Buffrenil, V., Castanet, J., Geraudie, J., Meunier, F.J., Sire, J.Y. et al. (1990) Microstructure and mineralization of vertebrate skeletal tissues. In: Carter, J.G. (Ed.) *Skeletal biomineralization: patterns, processes, and evolutionary trends*, Vol. 1. New York, NY: Van Nostrand Reinhold, pp. 471–548.
- Freedman Fowler, E.A. & Horner, J.R. (2015) A new brachylophosaurin hadrosaur (Dinosauria: Ornithischia) with an intermediate nasal crest from the Campanian Judith River formation of northcentral Montana. *PLoS ONE*, 10(11), e0141304. <https://doi.org/10.1371/journal.pone.0141304>
- Gangloff, R.A. & Fiorillo, A.R. (2010) Taphonomy and paleoecology of a bonebed from the Prince Creek formation, north slope, Alaska. *PALAIOS*, 25(5–6), 299–317.
- Hall, B.K. (2015) *Bones and cartilage: developmental and evolutionary skeletal biology*. Amsterdam: Academic Press, pp. 1–920.
- Holland, B., Bell, P.R., Fanti, F., Hamilton, S.M., Larson, D.W., Sissons, R. et al. (2021) Taphonomy and taxonomy of a juvenile lambeosaurine (Ornithischia: Hadrosauridae) bonebed from the late Campanian wapiti formation of northwestern Alberta, Canada. *PeerJ*, 9, e11290. <https://doi.org/10.7717/peerj.11290>
- Hone, D.W.E., Sullivan, C., Zhao, Q., Wang, K. & Xu, X. (2014) Body size distribution in a death assemblage of a colossal hadrosaurid from the upper cretaceous of Zhucheng, Shandong Province, China. In: Eberth, D.A. & Evans, D.C. (Eds.) *Hadrosaurs*. Bloomington, IN: Indiana University Press, pp. 524–531.
- Horner, J.R. (1982) Evidence of colonial nesting and 'site fidelity' among ornithischian dinosaurs. *Nature*, 297(5868), 675–676. <https://doi.org/10.1038/297675ao>
- Horner, J.R. (1999) Egg clutches and embryos of two hadrosaurian dinosaurs. *Journal of Vertebrate Paleontology*, 19(4), 607–611.
- Horner, J.R., de Ricqlès, A. & Padian, K. (1999) Variation in dinosaur skeletochronology indicators: implications for age assessment and physiology. *Paleobiology*, 25(3), 295–304. <https://doi.org/10.1017/S0094837300021308>
- Horner, J.R., de Ricqlès, A. & Padian, K. (2000) Long bone histology of the hadrosaurid dinosaur *Maiasaura peeblesorum*: growth dynamics and physiology based on an ontogenetic series of skeletal elements. *Journal of Vertebrate Paleontology*, 20(1), 115–129. [https://doi.org/10.1671/0272-4634\(2000\)020\[0115:LBHOTH\]2.0.CO;2](https://doi.org/10.1671/0272-4634(2000)020[0115:LBHOTH]2.0.CO;2)
- Horner, J.R. & Makela, R. (1979) Nest of juveniles provides evidence of family structure among dinosaurs. *Nature*, 282(5736), 296–298. <https://doi.org/10.1038/282296a0>
- Horner, J.R. & Padian, K. (2004) Age and growth dynamics of *Tyrannosaurus rex*. *Proceedings of the Royal Society of London B*, 271(1551), 1874–1880.
- Horner, J.R., Weishampel, D.B. & Forster, C.A. (2004) Hadrosauridae. In: Weishampel, D.B., Dodson, P. & Osmólska, H. (Eds.) *The Dinosauria*. Berkeley, CA: University of California Press, pp. 438–463.
- Hübner, T.R. (2012) Bone histology in *Dysalotossaurus lettowvorbecki* (Ornithischia: Iguanodontia) – variation, growth, and implication. *PLoS ONE*, 7, e22958.
- Huttenlocker, A.K., Woodward, H. & Hall, B.K. (2013) The biology of bone. In: Padian, K. & Lamm, E.-T. (Eds.) *Bone histology of fossil tetrapods: advancing methods, analysis, and interpretation*. Berkeley, CA: University of California Press, pp. 13–34.
- Köhler, M., Marin-Moratalla, N., Jordana, X. & Aanes, R. (2012) Seasonal bone growth and physiology in endotherms shed light on dinosaur physiology. *Nature*, 487(7407), 358–361. <https://doi.org/10.1038/nature11264>
- Lamm, E.-T. (2013) Preparation and sectioning of specimens. In: Padian, K. & Lamm, E.-T. (Eds.) *Bone histology of fossil tetrapods: advancing methods, analysis, and interpretation*. Berkeley, CA: University of California Press, pp. 55–160.



- Lauters, P., Bolotsky, Y.L., van Itterbeeck, J. & Godefroit, P. (2008) Taphonomy and age profile of a latest cretaceous dinosaur bone bed in far eastern Russia. *PALAIOS*, 23(3), 153–162. <https://doi.org/10.2110/palo.2006.p06-031r>
- Lee, A.H. & O'Connor, P.M. (2013) Bone histology confirms determinate growth and small body size in the noasaurid theropod *Masiakasaurus knopfleri*. *Journal of Vertebrate Paleontology*, 33(4), 865–876. <https://doi.org/10.1080/02724634.2013.743898>
- Lengendre, P. (2013). Model II regression. Version 1.6–3. CRAN.
- Marsh, O.C. (1892) Notice of new reptiles from the Laramie formation. *American Journal of Science*, Series 3 XLIII, 449–453. <https://doi.org/10.2475/ajs.s3-43.257.449>
- Mumby, H.S., Mar, K.U., Hayward, A.D., Htut, W., Htut-Aung, T. & Lummaa, V. (2015) Elephants born in the high stress season have faster reproductive ageing. *Scientific Reports*, 5(1), 13946. <https://doi.org/10.1038/srep13946>
- Nelms, L.G. (1989) Late cretaceous dinosaurs from the north slope of Alaska. *Journal of Vertebrate Paleontology*, Program and Abstracts, 34A.
- Olson, E.C. (1957) Size-frequency distributions in samples of extinct organisms. *Journal of Geology*, 65(3), 309–333. <https://doi.org/10.1086/626432>
- Padian, K. (2013) Why study the bone microstructure of fossil tetrapods? In: Padian, K. & Lamm, E.-T. (Eds.) *Bone histology of fossil tetrapods: advancing methods, analysis, and interpretation*. Berkeley, CA: University of California Press, pp. 1–12.
- R-Development-Core-Team. (2016) *R: a language and environment for statistical computing*, 3.3.1 edition. Vienna, Austria: R Foundation for Statistical Computing.
- Reid, R.E.H. (1985) On supposed Haversian bone from the hadrosaur *Anatosaurus*, and the nature of compact bone in dinosaurs. *Journal of Paleontology*, 59(1), 140–148.
- Rogers, R.R. & Kidwell, S.M. (2007) A conceptual framework for the genesis and analysis of vertebrate skeletal concentrations. In: Rogers, R.R., Eberth, D.A. & Fiorillo, A.R. (Eds.) *Bonebeds: Genesis, analysis, and paleobiological significance*. Chicago: University of Chicago Press, pp. 1–64.
- Scherzer, B.A. & Varricchio, D.J. (2010) Taphonomy of a juvenile lambeosaurine bonebed from the two medicine formation (Campanian) of Montana, United States. *PALAIOS*, 25(12), 780–795. <https://doi.org/10.2110/palo.2009.p09-143r>
- Shimazaki, H. & Shinomoto, S. (2007) A method for selecting the bin size of a time histogram. *Neural Computation*, 19(6), 1503–1527. <http://doi.org/10.1162/neco.2007.19.6.1503>
- Shimazaki, H. & Shinomoto, S. (2010) Kernel bandwidth optimization in spike rate estimation. *Journal of Computational Neuroscience*, 29(1), 171–182. <http://doi.org/10.1007/s10827-009-0180-4>
- Snyder, K., McLain, M., Wood, J., Chadwick, A. (2020) Over 13,000 elements from a single bonebed help elucidate disarticulation and transport of an *Edmontosaurus* thanatocoenosis. *PLOS ONE*, 15(5), e0233182. <https://doi.org/10.1371/journal.pone.0233182>
- Ullmann, P.V., Shaw, A., Nelleremoe, R. & Lacovara, K.J. (2017) Taphonomy of the standing rock hadrosaur site, Corson County, South Dakota. *PALAIOS*, 32(12), 779–796. <https://doi.org/10.2110/palo.2017.060>
- Vandervyn, E., Burns, M.E. & Currie, P.J. (2014) Histologic growth dynamic study of *Edmontosaurus regalis* (Dinosauria: Hadrosauridae) from a bonebed assemblage of the upper cretaceous horseshoe canyon formation, Edmonton, Alberta, Canada. *Canadian Journal of Earth Sciences*, 51(11), 1023–1033. <https://doi.org/10.1139/cjes-2014-0064>
- Varricchio, D.J. & Horner, J.R. (1993) Hadrosaurid and lambeosaurid bone beds from the upper cretaceous two medicine formation of Montana: Taphonomic and biologic implications. *Canadian Journal of Earth Sciences*, 30(5), 997–1006. <https://doi.org/10.1139/e93-083>
- Voorhies, M.R. (1969) Taphonomy and population dynamics of an Early Pliocene vertebrate fauna, Knox County, Nebraska. *Contribution to Geology*, Special Paper No., 1, 1–69.
- Woodward, H.N., Freedman Fowler, E.A., Farlow, J.O. & Horner, J.R. (2015) *Maiasaura*, a model organism for extinct vertebrate population biology: a large sample statistical assessment of growth dynamics and survivorship. *Paleobiology*, 41(4), 503–527. <https://doi.org/10.1017/pab.2015.19>
- Woodward, H.N., Horner, J.R. & Farlow, J.O. (2011) Osteohistological evidence for determinate growth in the American alligator. *Journal of Herpetology*, 45(3), 339–342. <https://doi.org/10.1670/10-274.1>
- Woodward, H.N., Padian, K. & Lee, A.H. (2013) Skeletochronology. In: Padian, K. & Lamm, E.-T. (Eds.) *Bone histology of fossil tetrapods: advancing methods, analysis, and interpretation*. Berkeley, CA: University of California Press, pp. 195–216.
- Wosik, M., Chiba, K., Therrien, F. & Evans, D.C. (2020) Testing size-frequency distributions as a method of ontogenetic aging: a life-history assessment of hadrosaurid dinosaurs from the Dinosaur Park formation of Alberta, Canada, with implications for hadrosaurid paleoecology. *Paleobiology*, 46(3), 379–404. <https://doi.org/10.1017/pab.2020.2>
- Wosik, M., Goodwin, M.B. & Evans, D.C. (2017) A nestling-sized skeleton of *Edmontosaurus* (Ornithischia, Hadrosauridae) from the Hell Creek formation of northeastern Montana, USA, with an analysis of ontogenetic limb allometry. *Journal of Vertebrate Paleontology*, 37(6), e1398168. <https://doi.org/10.1080/02724634.2017.1398168>
- Wosik, M., Goodwin, M.B. & Evans, D.C. (2019) Nestling-sized hadrosaurine cranial material from the Hell Creek formation of northeastern Montana, USA, with an analysis of cranial ontogeny in *Edmontosaurus annectens*. *PaleoBios*, 36, 1–18.
- Wosik, M., Whitney, M.R., Curry Rogers, K., Woodward, H. & Evans, D.C. (2017) Defining dinosaur neonatal body size using osteohistological evidence. In: Pellegrini, R.A. & Parris, D.C. (Eds.) *Fourth international symposium on paleohistology*. New Jersey State Museum: Trenton, NJ, p. 36.
- Wosik, M., Whitney, M.R., Curry Rogers, K., Woodward, H. & Evans, D.C. (2018) Defining dinosaur neonatal body size using osteohistological evidence. *Journal of Vertebrate Paleontology*, Program and Abstracts, 244.
- Xing, H., Mallon, J.C. & Currie, M.L. (2017) Supplementary cranial description of the types of *Edmontosaurus regalis* (Ornithischia: Hadrosauridae), with comments on the phylogenetics and biogeography of Hadrosaurinae. *PLoS ONE*, 12(4), e0175253. <https://doi.org/10.1371/journal.pone.0175253>
- Xing, H., Zhao, X., Wang, K., Li, D., Chen, S., Mallon, J.C. et al. (2014) Comparative osteology and phylogenetic relationships of *Edmontosaurus* and *Shantungosaurus* (Dinosauria: Hadrosauridae) from the upper cretaceous of North America and East Asia. *Acta Geologica Sinica*, 88(6), 1623–1652. <https://doi.org/10.1111/1755-6724.12334>

## SUPPORTING INFORMATION

Additional supporting information can be found online in the Supporting Information section at the end of this article.

### How to cite this article: Wosik, M. & Evans, D.C. (2022)

Osteohistological and taphonomic life-history assessment of *Edmontosaurus annectens* (Ornithischia: Hadrosauridae) from the Late Cretaceous (Maastrichtian) Ruth Mason dinosaur quarry, South Dakota, United States, with implication for ontogenetic segregation between juvenile and adult hadrosaurids. *Journal of Anatomy*, 241, 272–296. <https://doi.org/10.1111/joa.13679>